

SUBARU HIGH-*z* EXPLORATION OF LOW-LUMINOSITY QUASARS (SHELLQs). IV. DISCOVERY OF 41 QUASARS AND LUMINOUS GALAXIES AT $5.7 \leq z \leq 6.9$

YOSHIKI MATSUOKA,¹ KAZUSHI IWASAWA,² MASAFUSA ONOUE,^{3,4} NOBUNARI KASHIKAWA,^{3,4} MICHAEL A. STRAUSS,⁵ CHIEN-HSIU LEE,⁶ MASATOSHI IMANISHI,^{3,4} TOHRU NAGAO,¹ MASAYUKI AKIYAMA,⁷ NAOKO ASAMI,⁸ JAMES BOSCH,⁵ HISANORI FURUSAWA,³ TOMOTSUGU GOTO,⁹ JAMES E. GUNN,⁵ YUICHI HARIKANE,^{10,11} HIROYUKI IKEDA,³ TAKUMA IZUMI,³ TOSHIHIRO KAWAGUCHI,¹² NANAKO KATO,¹³ SATOSHI KIKUTA,^{3,4} KOTARO KOHNO,^{14,15} YUTAKA KOMIYAMA,^{3,4} ROBERT H. LUPTON,⁵ TAKEO MINEZAKI,¹⁴ SATOSHI MIYAZAKI,^{3,4} TOMOKI MOROKUMA,¹⁴ HITOSHI MURAYAMA,¹⁶ MANA NIIDA,¹³ ATSUSHI J. NISHIZAWA,¹⁷ MASAMUNE OGURI,^{11,16,15} YOSHIKI ONO,¹⁰ MASAMI OUCHI,^{10,16} PAUL A. PRICE,⁵ HIROAKI SAMESHIMA,¹⁸ ANDREAS SCHULZE,³ HIKARI SHIRAKATA,¹⁹ JOHN D. SILVERMAN,²⁰ NAOSHI SUGIYAMA,^{20,21} PHILIP J. TAIT,⁶ MASAHIRO TAKADA,¹⁶ TADAFUMI TAKATA,^{3,4} MASAYUKI TANAKA,^{3,4} JI-JIA TANG,²² YOSHIKI TOBA,^{1,22,23} YOUSUKE UTSUMI,²⁴ SHIANG-YU WANG,²² AND TAKUJI YAMASHITA¹

¹Research Center for Space and Cosmic Evolution, Ehime University, Matsuyama, Ehime 790-8577, Japan.

²ICREA and Institut de Ciències del Cosmos, Universitat de Barcelona, IEEC-UB, Martí i Franquès, 1, 08028 Barcelona, Spain.

³National Astronomical Observatory of Japan, Mitaka, Tokyo 181-8588, Japan.

⁴Department of Astronomical Science, Graduate University for Advanced Studies (SOKENDAI), Mitaka, Tokyo 181-8588, Japan.

⁵Princeton University Observatory, Peyton Hall, Princeton, NJ 08544, USA.

⁶Subaru Telescope, Hilo, HI 96720, USA.

⁷Astronomical Institute, Tohoku University, Aoba, Sendai, 980-8578, Japan.

⁸Seisa University, Hakone-machi, Kanagawa, 250-0631, Japan.

⁹Institute of Astronomy and Department of Physics, National Tsing Hua University, Hsinchu 30013, Taiwan.

¹⁰Institute for Cosmic Ray Research, The University of Tokyo, Kashiwa, Chiba 277-8582, Japan

¹¹Department of Physics, Graduate School of Science, The University of Tokyo, Bunkyo, Tokyo 113-0033, Japan

¹²Department of Economics, Management and Information Science, Onomichi City University, Onomichi, Hiroshima 722-8506, Japan.

¹³Graduate School of Science and Engineering, Ehime University, Matsuyama, Ehime 790-8577, Japan.

¹⁴Institute of Astronomy, The University of Tokyo, Mitaka, Tokyo 181-0015, Japan.

¹⁵Research Center for the Early Universe, University of Tokyo, Tokyo 113-0033, Japan.

¹⁶Kavli Institute for the Physics and Mathematics of the Universe, WPI, The University of Tokyo, Kashiwa, Chiba 277-8583, Japan.

¹⁷Institute for Advanced Research, Nagoya University, Furo-cho, Chikusa-ku, Nagoya 464-8602, Japan.

¹⁸Koyama Astronomical Observatory, Kyoto-Sangyo University, Kita, Kyoto, 603-8555, Japan.

¹⁹Department of CosmoSciences, Graduates School of Science, Hokkaido University, Kitaku, Sapporo 060-0810, Japan.

²⁰Kavli Institute for the Physics and Mathematics of the Universe, WPI, The University of Tokyo, Kashiwa, Chiba 277-8583, Japan.

²¹Graduate School of Science, Nagoya University, Furo-cho, Chikusa-ku, Nagoya 464-8602, Japan.

²²Institute of Astronomy and Astrophysics, Academia Sinica, Taipei, 10617, Taiwan.

²³Department of Astronomy, Kyoto University, Kitashirakawa-Oiwake-cho, Sakyo-ku, Kyoto 606-8502, Japan.

²⁴Kavli Institute for Particle Astrophysics and Cosmology, Stanford University, CA 94025, USA.

Submitted to ApJ

ABSTRACT

We report discovery of 41 new high-*z* quasars and luminous galaxies, which were spectroscopically identified at $5.7 \leq z \leq 6.9$. This is the fourth in a series of papers from the Subaru High-*z* Exploration of Low-Luminosity Quasars (SHELLQs) project, based on the deep multi-band imaging data collected by the Hyper Suprime-Cam (HSC) Subaru Strategic Program survey. We selected the photometric candidates by a Bayesian probabilistic algorithm, and then

carried out follow-up spectroscopy with the Gran Telescopio Canarias and the Subaru Telescope. Combined with the sample presented in the previous papers, we have now spectroscopically identified 137 extremely-red HSC sources over about 650 deg^2 , which include 64 high- z quasars, 24 high- z luminous galaxies, 6 [O III] emitters at $z \sim 0.8$, and 43 Galactic cool dwarfs (low-mass stars and brown dwarfs). The new quasars span the luminosity range from $M_{1450} \sim -26$ to -22 mag, and continue to populate a few magnitude lower luminosities than have been probed by previous wide-field surveys. In a companion paper, we derive the quasar luminosity function at $z \sim 6$ over an unprecedentedly wide range of $M_{1450} \sim -28$ to -21 mag, exploiting the SHELLQs and other survey outcomes.

Keywords: dark ages, reionization, first stars — galaxies: active — galaxies: high-redshift — intergalactic medium — quasars: general — quasars: supermassive black holes

1. INTRODUCTION

High- z quasars¹ are an important probe of the early Universe in many aspects. Their rest-ultraviolet (UV) spectra bluewards of Ly α are very sensitive to the H I absorption, and thus indicate the progress of cosmic reionization through the neutral fraction of the intergalactic medium (IGM; Gunn & Peterson 1965; Fan et al. 2006a). The very existence of such objects puts strong restriction on, and sometimes even challenges, models of formation and early evolution of supermassive black holes (SMBH; e.g., Volonteri 2012; Ferrara et al. 2014; Madau et al. 2014). High- z quasars are also used to probe the assembly of the host galaxies, which are thought to form in the highest density peaks of the dark matter distribution in the early phase of cosmic history (e.g., Goto et al. 2009; Decarli et al. 2017).

Previous surveys have identified more than 100 high- z quasars so far (e.g., Bañados et al. 2016, and references therein), with the most distant objects known at $z = 7.54$ (Bañados et al. 2018) and $z = 7.085$ (Mortlock et al. 2011). However, most of the known quasars have redshifts $z < 6.5$ and UV absolute magnitudes $M_{1450} < -24$ mag, while higher redshifts and fainter magnitudes remain largely unexplored. There must be numerous objects of faint quasars and active galactic nuclei (AGNs) behind the known luminous quasars; they may represent the more typical mode of SMBH growth in the early Universe, and may have made a significant contribution to reionization.

For the past few years, we have been carrying out a high- z quasar survey with the Subaru 8.2-m telescope. We have already reported discovery of 33 high- z quasars, along with 14 high- z luminous galaxies, 2 [O III] emitters at $z \sim 0.8$, and 15 Galactic brown dwarfs, in Matsuoka et al. (2016, 2018, Paper I and II, hereafter). Multi-wavelength follow-up observations of the discovered objects are ongoing, whose initial results from the Atacama Large Millimeter/ submillimeter Array (ALMA) data are presented in Izumi et al. (2018, Paper III). This “Subaru High- z Exploration of Low-Luminosity Quasars (SHELLQs)” project is based on the exquisite multi-band photometry data collected by the Hyper Suprime-Cam (HSC) Subaru Strategic Program (SSP) survey (Aihara et al. 2018b). HSC is a

wide-field camera on the Subaru Telescope, and has a nearly circular field of view of $1^\circ.5$ diameter, covered by $116\,2\text{K} \times 4\text{K}$ Hamamatsu fully depleted CCDs, with the pixel scale of $0''.17$ (Miyazaki et al. 2018). The camera dewar design and on-site quality assurance design are described in Komiyama et al. (2018) and Furusawa et al. (2018), respectively. The HSC-SSP survey has three layers with different combinations of area and depth. The Wide layer is observing $1400\,\text{deg}^2$ mostly along the celestial equator, with the 5σ point-source depths of $(g_{\text{AB}}, r_{\text{AB}}, i_{\text{AB}}, z_{\text{AB}}, y_{\text{AB}}) = (26.5, 26.1, 25.9, 25.1, 24.4)$ mag measured in $2''.0$ aperture. The Deep and the UltraDeep layers are observing smaller areas (27 and $3.5\,\text{deg}^2$) down to deeper limiting magnitudes ($r_{\text{AB}} = 27.1$ and 27.7 mag, respectively). The observed data are processed with the dedicated pipeline *hscPipe* (Bosch et al. 2018), which was developed from the Large Synoptic Survey Telescope software pipeline (Jurić et al. 2015). The HSC pipeline is evolving through the period of the survey, which sometimes gives rise to somewhat inconsistent photometry (and quasar probability of a given source; see below) between different data releases. A full description of the HSC-SSP survey may be found in Aihara et al. (2018b).

This paper is the fourth in a series of SHELLQs publications, and reports spectroscopic identification of an additional 73 objects in the latest HSC-SSP data. We describe the photometric candidate selection briefly in §2, while a more complete description may be found in Paper I and II. The spectroscopic follow-up observations are described in §3. The quasars and other classes of objects we discovered are presented in §4. A summary appears in §5. A companion paper (Y. Matsuoka et al., in prep.) describes the quasar luminosity function at $z \sim 6$ derived from the SHELLQs sample obtained so far. This paper adopts the cosmological parameters $H_0 = 70\,\text{km s}^{-1}\,\text{Mpc}^{-1}$, $\Omega_{\text{M}} = 0.3$, and $\Omega_{\Lambda} = 0.7$. All magnitudes in the optical and NIR bands are presented in the AB system (Oke & Gunn 1983), and are corrected for Galactic extinction (Schlegel et al. 1998). We use two types of magnitudes; the point spread function (PSF) magnitude (m_{AB}) is measured by fitting PSF models to the source profile, while the CModel magnitude ($m_{\text{CModel,AB}}$) is measured by fitting PSF-convolved, two-component galaxy models (Abazajian et al. 2004). We use the PSF magnitude error (σ_{m}) measured by the HSC data processing pipeline (Bosch et al. 2018); it does not contain photometric calibration uncertainty, which is estimated to be at least 1 % (Aihara et al. 2018a). In what follows, we refer to z -band magnitudes with the AB subscript (“ z_{AB} ”), while redshift z appears without a subscript.

¹ Throughout this paper, “high- z ” denotes $z > 5.7$, where quasars are observed as i -band dropouts in the Sloan Digital Sky Survey (SDSS) filter system (Fukugita et al. 1996). The term “ X -band dropouts” or “ X -dropouts” refers to objects which are much fainter in the X and bluer bands (and very often invisible) than in the redder bands.

2. PHOTOMETRIC CANDIDATE SELECTION

Our photometric candidate selection starts from the HSC-SSP source catalog. We used the survey data in the three layers, observed before 2017 May, i.e., a newer dataset than contained in the latest public data release (Aihara et al. 2018a). We require that our quasar survey field has been observed in the i , z , and y bands (not necessarily to the full depths; see below), but impose no requirement on the g - or r -band coverage. All sources meeting the following criteria, without critical quality flags (see Paper I), are selected:

$$(z_{AB} < 24.5 \text{ and } \sigma_z < 0.155 \text{ and } i_{AB} - z_{AB} > 1.5 \\ \text{and } z_{AB} - z_{\text{CModel},AB} < 0.15) \quad (1)$$

or

$$(y_{AB} < 24.0 \text{ and } \sigma_y < 0.155 \text{ and } z_{AB} - y_{AB} > 0.8 \\ \text{and } y_{AB} - y_{\text{CModel},AB} < 0.15). \quad (2)$$

Here we use the difference between the PSF and CModel magnitudes ($m_{AB} - m_{\text{CModel},AB}$) to reject extended sources. With the present threshold value (0.15), our completeness of point source selection is $>80\%$ at $z_{AB} < 24.0$ mag (Paper II). The completeness decreases toward fainter magnitude, which should be accounted for in statistical measurements (e.g., luminosity function) of the discovered quasars. We further remove sources with more than 3σ detection in the g or r band, if these bands are available, as such sources are most likely low- z interlopers.

Next, we process the HSC images of the above sources through an automatic image checking procedure, in all the available bands. As detailed in Paper I and II, this procedure uses Source Extractor (Bertin & Arnouts 1996), and removes those sources whose photometry is not consistent (within 5σ significance) between the stacked and all the pre-stacked, individual images. We also eliminate sources with too compact, diffuse, or elliptical profiles to be celestial point sources on the stacked images. The sources removed at this stage are mostly cosmic rays, moving or transient sources, or image artifacts.

The candidates selected above are matched, within $1''.0$ separation, to the public near-IR catalogs from the United Kingdom Infrared Telescope Infrared Deep Sky Survey (Lawrence et al. 2007), the Visible and Infrared Survey Telescope for Astronomy (VISTA) Kilo-degree Infrared Galaxy survey, the VISTA Deep Extragalactic Observations Survey (Jarvis et al. 2013), and the UltraVISTA survey (McCracken et al. 2012). The choice of the $1''.0$ matching radius is rather arbitrary, but is at least sufficiently larger than the astrometric uncertainties of the above surveys. Then using the i , z and

y -band magnitudes along with all the available J , H , and/or K magnitudes, we calculate Bayesian quasar probability (P_Q^B) for each candidate, based on spectral energy distribution (SED) models and estimated surface densities of high- z quasars and contaminating brown dwarfs as a function of magnitude. Our algorithm does not contain galaxy models at present. We created the quasar SED models by stacking the SDSS spectra of 340 bright quasars at $z \simeq 3$, where the quasar color selection is fairly complete (Richards et al. 2002; Willott et al. 2005), and correcting for the effect of IGM absorption (Songaila 2004). The quasar surface density was modeled with the luminosity function of Willott et al. (2010). The color models of brown dwarfs were computed with a set of observed spectra compiled in the SpeX prism library² and the CGS4 library³, while the surface densities were calculated following Caballero et al. (2008). A more detailed description of our Bayesian algorithm may be found in Paper I. We reject sources with $P_Q^B < 0.1$, and keep those with higher quasar probability in the sample of candidates.

Finally, we inspect the images of all the candidates by eye and remove additional problematic sources. About 80 % of the remaining candidates were rejected at this last stage, which are mostly cosmic rays but also include transient/moving objects and sources close to bright stars. The latest HSC-SSP (internal) data release covers 650 deg^2 , when we limit to the field where at least a single exposure in the i and two exposures each in the z and y bands were obtained. From the final sample of candidates, we put the highest priority for spectroscopic identification on a subsample with relatively bright magnitudes ($z_{AB} < 24.0$ mag or $y_{AB} < 23.5$ mag), red colors ($i_{AB} - z_{AB} > 2.0$ or $z_{AB} - y_{AB} > 0.8$), and detection in more than a single band (for i -dropouts) or a single exposure (for z -dropouts). The number of our photometric candidates is changing throughout the survey, due to continuous arrival of new HSC-SSP survey data, a change in the photometry and quasar probability (P_Q^B) with updates of the data processing pipeline, and the progress of our follow-up spectroscopy.

The present HSC survey footprint includes 15 high- z quasars discovered by other surveys, as summarized in Table 1. We recovered ten of these quasars with $P_Q^B = 1.000$, while three quasars were not selected due to their relatively low redshifts ($z < 5.9$) and bluer HSC colors ($i_{AB} - z_{AB} < 1.5$) than the HSC color selection threshold described above. The remaining two quasars are missing

² <http://pono.ucsd.edu/~adam/browndwarfs/spexprism>

³ <http://staff.gemini.edu/~sleggett/LTdata.html>

due to nearby bright sources; VIK $J0839 + 0015$ is assigned with an HSC `pixelflags_bright_objectcenter` flag (indicating that the pipeline measurements of this source may be affected by a nearby bright source) and therefore does not meet the HSC source selection criteria described above, while SDSS $J1602 + 4228$ is rejected in our automatic image checking procedure, since its *i*-band photometry is not consistent between stacked and pre-stacked images, likely due to blending with a foreground galaxy.

3. SPECTROSCOPY

Our previous papers reported the results of follow-up spectroscopy carried out before 2016 Autumn. Since that time, we have observed 73 additional quasar candidates, using the Optical System for Imaging and low-Intermediate-Resolution Integrated Spectroscopy (OSIRIS; Cepa et al. 2000) mounted on the 10.4-m Gran Telescopio Canarias (GTC), and the Faint Object Camera and Spectrograph (FOCAS; Kashikawa et al. 2002) mounted on Subaru. We observed roughly the brightest one-third of the candidates with OSIRIS, and the remaining candidates with FOCAS. The observations were scheduled in such a way that the targets with brighter magnitudes and higher P_Q^B were observed at the earlier opportunities. The journal of these discovery observations is presented in Table 2. We present the details of these observations below.

3.1. GTC/OSIRIS

GTC is a 10.4-m telescope located at the Observatorio del Roque de los Muchachos in La Palma, Spain. Our program was awarded 26 hours in the 2017A semester (GTC8-17A; Iwasawa et al.). We used OSIRIS with the R2500I grism and $1''.0$ -wide long slit, which provides spectral coverage from $\lambda_{\text{obs}} = 0.74$ to $1.0 \mu\text{m}$ with a resolution $R \sim 1500$. The observations were carried out in queue mode on dark and gray nights, with mostly photometric (sometimes spectroscopic) sky conditions and the seeing $0''.7 - 1''.3$. The data were reduced using the Image Reduction and Analysis Facility (IRAF). Bias correction, flat fielding with dome flats, sky subtraction, and 1d extraction were performed in the standard way. The wavelength calibration was performed with reference to sky emission lines. The flux calibration was tied to white dwarfs (Ross 640, Feige 110, G191-B2B) or a B-type standard star (HILT 600), observed as standard stars within a few days of the target observations. The slit losses were corrected for by scaling the spectra to match the HSC magnitudes in the *z* and *y* bands for the *i*- and *z*-band dropouts, respectively.

3.2. Subaru/FOCAS

Our program was awarded five nights each in the S17A and S17B semesters, as a part of a Subaru intensive program (S16B-071I; Matsuoka et al.). We used FOCAS in the multi-object spectrograph (MOS) mode with the VPH900 grism and SO58 order-sorting filter. The widths of the slitlets were set to $1''.0$. This configuration provides spectral coverage from $\lambda_{\text{obs}} = 0.75$ to $1.05 \mu\text{m}$ with a resolution $R \sim 1200$. The only exception is $J1400 + 0106$, which was observed with a $2''.0$ -wide longslit with the same grism and filter as the MOS observations. All the observations were carried out on gray nights. A few of these nights were occasionally affected by cirrus or poor seeing, while the weather was fairly good with seeing $0''.4 - 1''.2$ for the rest of the observations.

The data were reduced with IRAF using the dedicated FOCASRED package. Bias correction, flat fielding with dome flats, sky subtraction, and 1d extraction were performed in the standard way. The wavelength was calibrated with reference to the sky emission lines. The flux calibration was tied to white dwarf standard stars (G191-B2B, Feige 110, or GD 153) observed during the same run, in most cases on the same nights as the targets. The slit losses were corrected for in the same way as in the OSIRIS data reductions.

Table 1. Recovery of Known High- z Quasars

Name	R.A.	Decl.	Redshift	Recovered?	Comment
CFHQS <i>J</i> 0210 – 0456	02 ^h 10 ^m 13 ^s .19	–04°56′20″.9	6.43	Y	$P_Q^B = 1.000$
CFHQS <i>J</i> 0216 – 0455	02 ^h 16 ^m 27 ^s .81	–04°55′34″.1	6.01	Y	$P_Q^B = 1.000$
CFHQS <i>J</i> 0227 – 0605	02 ^h 27 ^m 43 ^s .29	–06°05′30″.2	6.20	Y	$P_Q^B = 1.000$
SDSS <i>J</i> 0836 + 0054	08 ^h 36 ^m 43 ^s .86	+00°54′53″.3	5.81	N	$i_{AB} - z_{AB} < 1.5$
VIK <i>J</i> 0839 + 0015	08 ^h 39 ^m 55 ^s .36	+00°15′54″.2	5.84	N	Close to a bright source
VIK <i>J</i> 1148 + 0056	11 ^h 48 ^m 33 ^s .18	+00°56′42″.3	5.84	N	$i_{AB} - z_{AB} < 1.5$
VIK <i>J</i> 1215 + 0023	12 ^h 15 ^m 16 ^s .87	+00°23′24″.7	5.93	Y	$P_Q^B = 1.000$
PSO <i>J</i> 184.3389 + 01.5284	12 ^h 17 ^m 21 ^s .34	+01°31′42″.5	6.20	Y	$P_Q^B = 1.000$
SDSS <i>J</i> 1602 + 4228	16 ^h 02 ^m 53 ^s .98	+42°28′24″.9	6.09	N	Blended with a foreground galaxy
IMS <i>J</i> 2204 + 0012	22 ^h 04 ^m 17 ^s .92	+01°11′44″.8	5.94	Y	$P_Q^B = 1.000$
VIMOS 2911001793	22 ^h 19 ^m 17 ^s .22	+01°02′48″.9	6.16	Y	$P_Q^B = 1.000$
SDSS <i>J</i> 2228 + 0110	22 ^h 28 ^m 43 ^s .54	+01°10′32″.2	5.95	Y	$P_Q^B = 1.000$
CFHQS <i>J</i> 2242 + 0334	22 ^h 42 ^m 37 ^s .55	+03°34′21″.6	5.88	N	$i_{AB} - z_{AB} < 1.5$
SDSS <i>J</i> 2307 + 0031	23 ^h 07 ^m 35 ^s .35	+00°31′49″.4	5.87	Y	$P_Q^B = 1.000$
SDSS <i>J</i> 2315 – 0023	23 ^h 15 ^m 46 ^s .57	–00°23′58″.1	6.12	Y	$P_Q^B = 1.000$

NOTE—The naming convention follows Bañados et al. (2016).

Table 2. Journal of Discovery Spectroscopy

Target	t_{exp} (min)	Date	Inst	Target	t_{exp} (min)	Date	Inst	Target	t_{exp} (min)	Date	Inst
<i>J2210 + 0304</i>	210	Sep 29, Oct 1	F	<i>J0858 + 0000</i>	15	Mar 1	O	<i>J0225 − 0351</i>	23	Oct 1	F
<i>J0213 − 0626</i>	80	Sep 28, Oct 1	F	<i>J0220 − 0432</i>	70	Sep 30	F	<i>J0837 − 0000</i>	15	Apr 23	O
<i>J0923 + 0402</i>	30	Mar 2	O	<i>J1422 + 0011</i>	30	May 3	F	<i>J0856 + 0248</i>	30	Mar 19	F
<i>J0921 + 0007</i>	15	Mar 1	O	<i>J2231 − 0035</i>	73	Sep 30	F	<i>J0900 + 0424</i>	40	Mar 18	F
<i>J1545 + 4232</i>	30	Mar 7	O	<i>J1209 − 0006</i>	60	Mar 17	F	<i>J0902 − 0030</i>	30	Mar 18	F
<i>J1004 + 0239</i>	30	Mar 18	F	<i>J1550 + 4318</i>	45	Mar 17	F	<i>J0906 − 0206</i>	45	Mar 1	O
<i>J0211 − 0203</i>	110	Sep 27, Oct 1	F	<i>J1428 + 0159</i>	30	Feb 15 (2018)	O	<i>J0906 + 0431</i>	45	Mar 18	F
<i>J2304 + 0045</i>	30	Sep 27	F	<i>J0917 − 0056</i>	120	Mar 2, Apr 23	O	<i>J0912 − 0121</i>	30	Mar 16	F
<i>J2255 + 0251</i>	90	Sep 27, Oct 1	F	<i>J0212 − 0315</i>	50	Sep 27	F	<i>J1359 + 0134</i>	30	Mar 18	F
<i>J1406 − 0116</i>	30	Mar 3	O	<i>J0212 − 0532</i>	50	Sep 29	F	<i>J1400 + 0106</i>	240	Mar 19	F
<i>J1146 − 0005</i>	60	Mar 7	O	<i>J2311 − 0050</i>	50	Sep 30	F	<i>J1415 − 0113</i>	15	Apr 23	O
<i>J1146 + 0124</i>	45	Mar 29	O	<i>J1609 + 5515</i>	80	Mar 17	F	<i>J1432 + 0045</i>	75	Mar 18	F
<i>J0918 + 0139</i>	60	Mar 2	O	<i>J1006 + 0300</i>	45	Mar 16	F	<i>J1434 − 0204</i>	15	Apr 22	O
<i>J0844 − 0132</i>	60	Dec 10	O	<i>J0914 + 0442</i>	50	Mar 19	F	<i>J1435 + 0040</i>	15	Apr 22	O
<i>J1146 − 0154</i>	60	Mar 31	O	<i>J0219 − 0132</i>	30	Sep 28	F	<i>J1607 + 5417</i>	30	Mar 18	F
<i>J0834 + 0211</i>	40	Dec 10	O	<i>J0915 − 0051</i>	75	Mar 18	F	<i>J1620 + 4438</i>	20	Mar 18	F
<i>J0909 + 0440</i>	15	Mar 1	O	<i>J1000 + 0211</i>	13	Mar 17	F	<i>J1629 + 4233</i>	30	May 3	F
<i>J2252 + 0225</i>	100	Sep 29, Oct 1	F	<i>J0154 − 0116</i>	14	Sep 28	F	<i>J2236 + 0006</i>	50	Sep 29	F
<i>J1406 − 0144</i>	60	Apr 22	O	<i>J2226 + 0237</i>	10	Sep 30	F	<i>J2239 − 0048</i>	25	Oct 1	F
<i>J1416 + 0147</i>	30	Apr 22	O	<i>J0845 − 0123</i>	10	Mar 16	F	<i>J2248 + 0103</i>	50	Sep 29	F
<i>J0957 + 0053</i>	75	Mar 16	F	<i>J0158 − 0033</i>	30	Sep 30	F	<i>J2253 − 0117</i>	40	Dec 14	O
<i>J2223 + 0326</i>	30	Sep 27	F	<i>J0207 − 0052</i>	10	Sep 27	F	<i>J2305 − 0051</i>	80	Sep 28	F
<i>J1400 − 0125</i>	50	Mar 16	F	<i>J0213 − 0334</i>	10	Sep 30	F	<i>J2315 − 0041</i>	25	Dec 22	O
<i>J1400 − 0011</i>	80	Mar 6, Apr 23	O	<i>J0216 − 0207</i>	30	Sep 30	F				
<i>J1219 + 0050</i>	30	Dec 22	O	<i>J0220 − 0134</i>	30	Sep 28	F				

NOTE—All the dates are in the year of 2017, except for *J1428 + 0159* observed in 2018. The instrument (Inst) “O” and “F” denote GTC/OSIRIS and Subaru/FOCAS, respectively.

4. RESULTS AND DISCUSSION

Figures 1 – 9 present the reduced spectra of the 73 candidates we observed. They include 31 high- z quasars, 10 high- z galaxies, 4 strong [O III] emitters at $z \sim 0.8$, and 28 cool dwarfs (low-mass stars and brown dwarfs). Their photometric properties are summarized in Table 3. The astrometric accuracy of the HSC-SSP data is estimated to be $\lesssim 0''.1$ (root mean square; Aihara et al. 2018a). Ten of these objects are detected in the J , H , and/or K band, as summarized in Table 4.

We identified 31 new quasars at $5.8 < z \leq 6.9$, as displayed in Figures 1 – 4 and listed in the first section of Table 5. The two highest- z quasars, $J2210 + 0304$ and $J0213 - 0626$ at $z = 6.9$ and $z = 6.72$, respectively, are observed as complete z -band dropouts on the HSC images. $J0923 + 0402$ has a very red $z - y$ color, but is clearly visible in the z band. All the remaining quasars are i -band dropouts. It is worth mentioning that we discovered two quasars at $z \sim 6.5$ ($J0921 + 0007$ and $J1545 + 4232$), where quasars have similar optical colors to Galactic brown dwarfs and are thus hard to identify (see Figure 1 of Paper II). These two quasars have very strong Ly α + N V $\lambda 1240$ lines, which allowed us to separate them from brown dwarfs due to their unusually blue $z - y$ colors.

The majority of the objects in Figures 1 – 4 exhibit characteristic spectral features of high- z quasars, namely, strong and broad Ly α and in some cases N V $\lambda 1240$, blue rest-UV continua, and sharp continuum breaks just blueward of Ly α . However, for some objects, the quality and wavelength coverage of our spectra are not sufficient to provide robust classification. In Paper I and II, we reported objects with luminous and narrow Ly α emission, whose quasar/galaxy classification is still ambiguous. Our new quasar sample also includes two such objects, namely, $J0220 - 0432$ and $J1209 - 0006$. Following Paper I and II, we classify these objects as possible quasars, due to their high Ly α luminosity ($L > 10^{43}$ erg s $^{-1}$). This is based on the fact that, at $z \sim 2$, the majority of Ly α emitters with $L > 10^{43}$ erg s $^{-1}$ are associated with AGNs, based on their X-ray, UV, and radio properties (Konno et al. 2016).

We estimated the redshifts of the discovered quasars from the Ly α lines, assuming that the observed line peaks correspond to the intrinsic Ly α wavelength (1216 Å in the rest frame). This assumption is not always correct, due to the strong H I absorption from the IGM. It is more difficult to measure redshifts of quasars without clear Ly α lines, as is the case for $J2210 + 0304$, $J0923 + 0402$, and several other quasars in our sample. In these cases we estimated rough redshifts from the wavelengths of the onset of the Gunn-Peterson trough.

Therefore, the redshifts presented here (Table 5) are accompanied by relatively large uncertainties (up to $\Delta z \sim 0.1$), and must be interpreted with caution. Future follow-up observations at other wavelengths, e.g., near-IR covering Mg II $\lambda 2800$ or sub-mm covering [C II] $158\mu\text{m}$, are crucial for secure redshift measurements.

The absolute magnitudes M_{1450} and Ly α line properties were measured in the same way as described in Paper II. For every object, we defined a continuum window at wavelengths relatively free from strong sky emission lines, and extrapolated the measured continuum flux to estimate M_{1450} . A power-law continuum model with a slope $\alpha = -1.5$ ($F_\lambda \propto \lambda^\alpha$; e.g., Vanden Berk et al. (2001)) was assumed. Since the continuum windows (falling in the range of $\lambda_{\text{rest}} = 1250 - 1350$ Å) are close to $\lambda_{\text{rest}} = 1450$ Å, these measurements are not sensitive to the exact value of α . Ly α properties (luminosity, FWHM, and rest-frame equivalent width [EW]) of an object with weak continuum emission, such as $J1146 - 0005$, was measured with a local continuum defined as an average flux of all the pixels redward of Ly α . For the remaining objects with relatively strong continuum, we measured the properties of the broad Ly α + N V complex, with a local continuum defined by the above power-law model. We didn't assume any line profile models, but used the continuum-subtracted flux counts directly to measure these line properties. Due to the difficulty in defining accurate continuum levels, these line measurements should be regarded as only approximate. The resultant line properties are summarized in Table 5. More detailed descriptions of the above procedure may be found in Paper II.

The ten objects without a broad or luminous ($> 10^{43}$ erg s $^{-1}$) Ly α line, as presented in Figure 5, are most likely galaxies at $z \sim 6$. We have now spectroscopically identified 24 such high- z luminous galaxies, when combined with the similar objects presented in the previous papers. Redshifts of these objects were estimated from the observed positions of Ly α emission, the interstellar absorption lines of Si II $\lambda 1260$, Si II $\lambda 1304$, C II $\lambda 1335$, and/or the continuum break caused by the IGM H I absorption. This is not always easy with our limited S/N, and hence the redshifts reported here must be regarded as only approximate (with uncertainties up to $\Delta z \sim 0.1$). The absolute magnitude M_{1450} and Ly α properties were measured in the same way as for quasars, except that we assumed a continuum slope of $\beta = -2.0$ ($F_\lambda \propto \lambda^\beta$; Stanway et al. 2005).

This paper also adds four [O III] emitters at $z \sim 0.8$ (see Figures 6) to the two similar objects reported in Paper II. We measured the line properties of H γ , H β , [O III] $\lambda 4959$ and $\lambda 5007$, and listed the results in Table

5. Since they have very weak continua, we estimated the continuum levels by summing up all the available pixels except for the above emission lines. This still gives relatively large uncertainties in the EWs for some of the objects. As we discussed in Paper II, their very high [O III] $\lambda 5007/H\beta$ ratios may indicate that these are galaxies with sub-solar metallicity and high ionization state of the interstellar medium (e.g., Kewley et al. 2016), and/or AGN contribution. J1000 + 0211 and J0845 – 0123 have extremely large [O III] $\lambda 5007$ EWs ($\gtrsim 5000$ Å), which even exceeds those found in the so-called “green pea” galaxies characterized by strong [O III] $\lambda 5007$ (EW $\lesssim 1000$ Å; Cardamone et al. 2009). These objects are clearly an interesting subject of future follow-up studies.

Finally, we found 28 new Galactic cool dwarfs (low-mass stars and brown dwarfs), as presented in Figures 7 – 9. We estimated their rough spectral classes by fitting the spectral standard templates of M4- to T8-type dwarfs, taken from the SpeX Prism Spectral Library (Burgasser 2014; Skrzypek et al. 2015), to the observed spectra at $\lambda = 7500 - 9800$ Å. The results are summarized in Table 6 and plotted in the figures. Due to the low S/N and limited wavelength coverage of the spectra, the classification presented here is accompanied by large uncertainties, and should be regarded as only approximate.

In Figure 10, we plot the HSC $i_{AB} - z_{AB}$ and $z_{AB} - y_{AB}$ colors of all the spectroscopically-identified objects in Paper I, II, and this work. We also include the ten previously-known quasars recovered by SHELLQs. The figure demonstrates that the discovered quasars broadly follow the expected colors from our SED model, while there are outliers with very blue $z_{AB} - y_{AB}$ colors, due to exceptionally large Ly α EWs. On the other hand, we are finding many cool dwarfs that are bluer than our fiducial models, due to the nature of our selection criteria. It may be worth noting a clump of brown dwarfs at $(i_{AB} - z_{AB}, z_{AB} - y_{AB}) \sim (3, 1)$; they lie exactly on the quasar SED track in the color space, and are thus assigned with high P_Q^B values as candidates of quasars at $z \sim 6.5$. The $z \sim 6$ galaxies occupy colors in between quasars and cool dwarfs, due to their weaker Ly α emission than quasars and bluer continua than cool dwarfs. Finally, the six [O III] emitters are well separated from the quasars on this diagram, and do not satisfy our latest selection condition of $i_{AB} - z_{AB} > 2.0$.

Figure 11 displays the redshifts versus absolute magnitudes M_{1450} of the SHELLQs quasars and galaxies, along with those of high- z quasars discovered by other surveys. We continue to probe a new parameter space at

$z > 5.7$ and $M_{1450} > -25$ mag, to which other surveys have only limited sensitivities.

Figure 12 presents a histogram of the Bayesian quasar probability (P_Q^B), for all the spectroscopically identified objects in Paper I, II, and this work. The P_Q^B values have a clear bimodal distribution, with the higher peak at $P_Q^B \sim 1.0$ being dominated by high- z quasars. All but one quasar have $P_Q^B > 0.8$, which implies that their spectral diversity is reasonably covered by the quasar model in our Bayesian algorithm. The lower peak at $P_Q^B \sim 0.0$ is populated mostly by cool dwarfs. Many of these dwarfs lie below the quasar selection threshold ($P_Q^B = 0.1$), due to the improvement of HSC photometry with updates of the data reduction pipeline; they were selected for spectroscopic identification because they had $P_Q^B > 0.1$ in the older data releases. This is also the case for the quasar J0220 – 0432, which had $z_{AB} - y_{AB} \sim 0.0$ and $P_Q^B = 1.0$ previously but happens to have $z_{AB} - y_{AB} \sim 0.4$ and $P_Q^B = 0.0$ in the latest data release. Because no additional z - or y -band data were taken for this object since the previous data release, and because this object is located within a few arcsec of a brighter galaxy, this discrepancy in color measurements may be due to different deblender treatment in the different versions of the HSC pipeline.

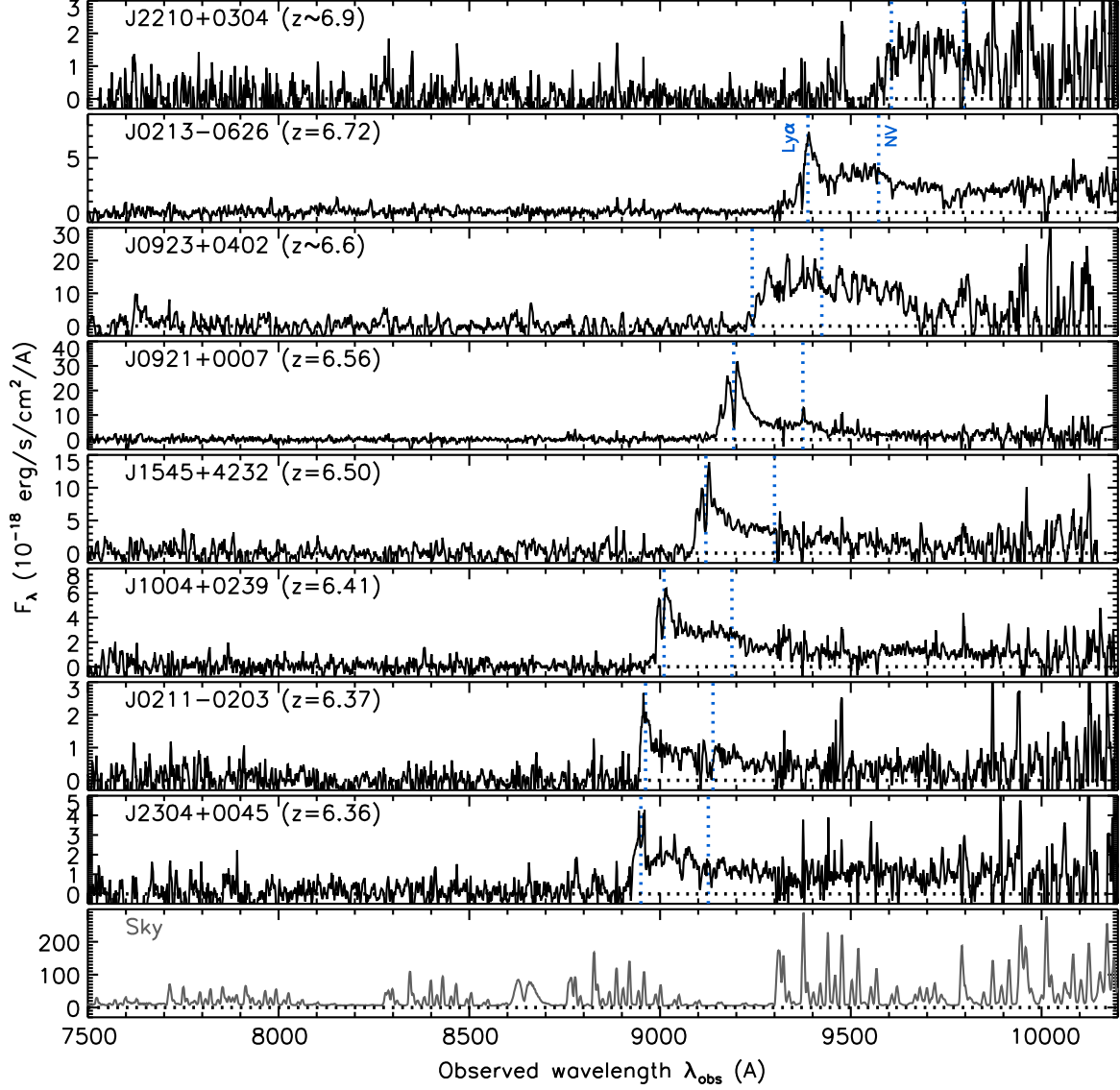


Figure 1. Reduced spectra of the first set of eight quasars discovered in this work, displayed in decreasing order of redshift. The object name and the estimated redshift are indicated at the top left corner of each panel. The blue dotted lines mark the expected positions of the Ly α and N V $\lambda 1240$ emission lines, given the redshifts. The spectra were smoothed using inverse-variance weighted means over 3 – 11 pixels (depending on the S/N), for display purposes. The bottom panel displays a sky spectrum, as a guide to the expected noise.

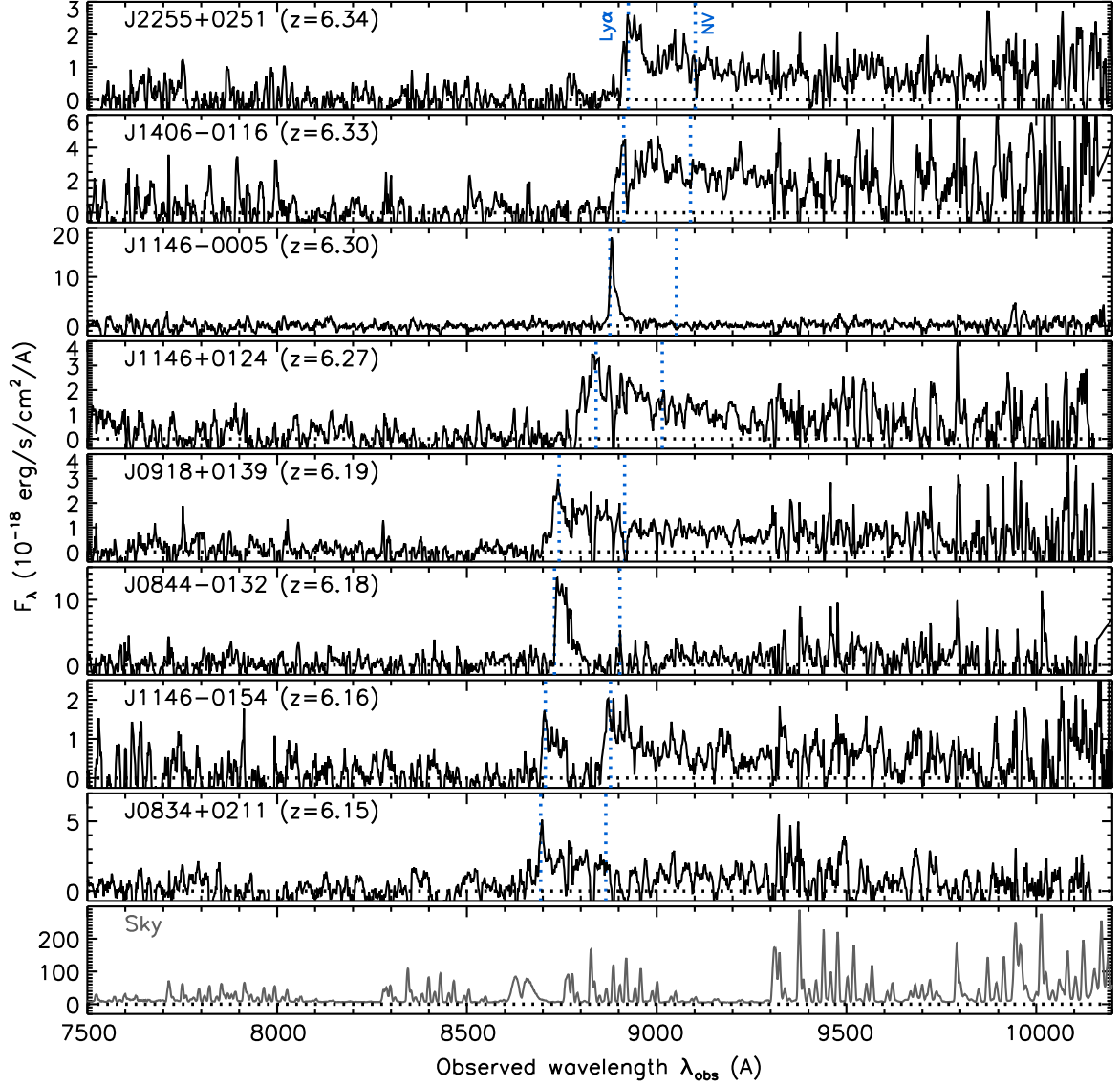


Figure 2. Same as Figure 1, but for the second set of eight quasars.

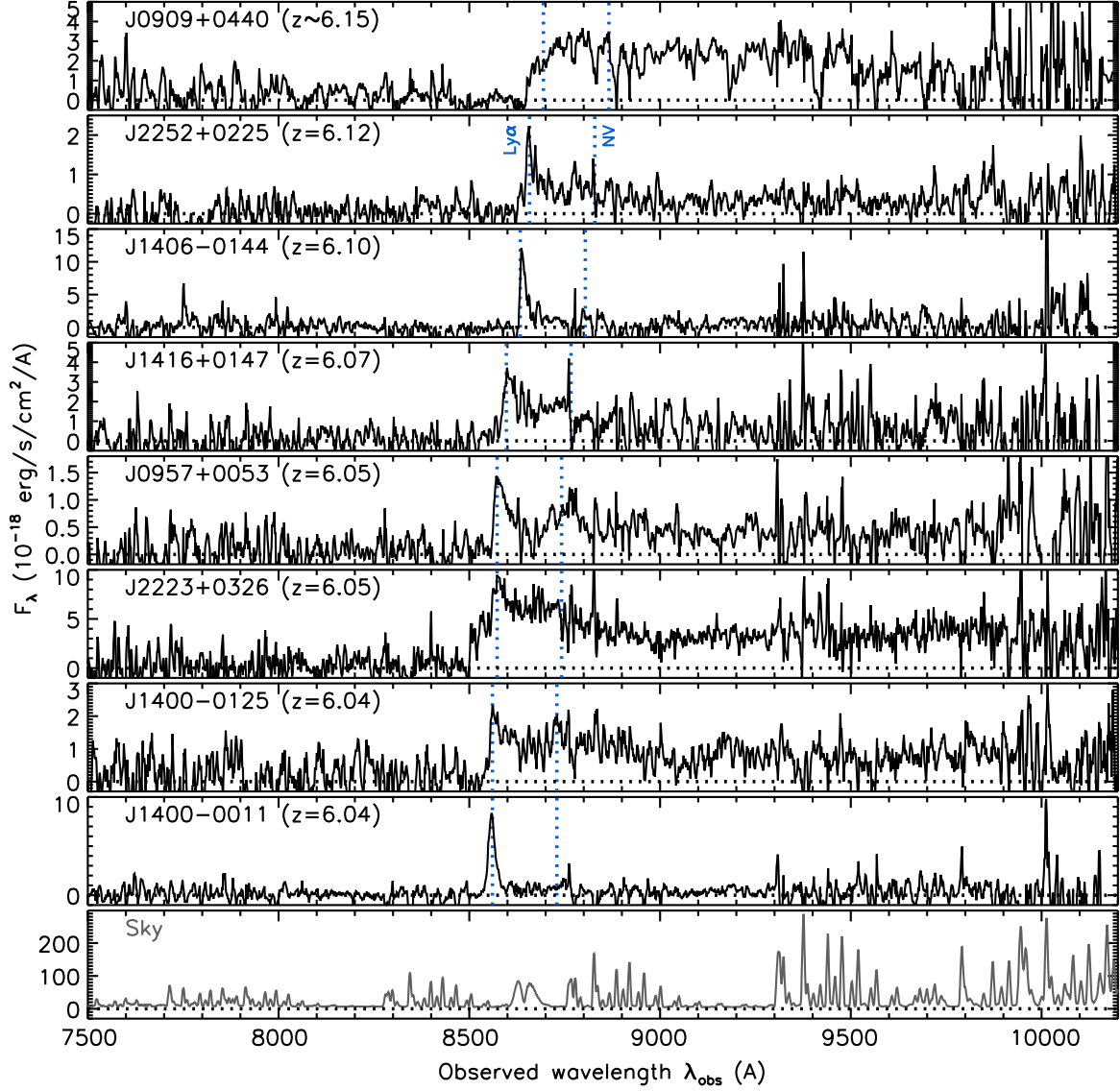


Figure 3. Same as Figure 1, but for the third set of eight quasars.

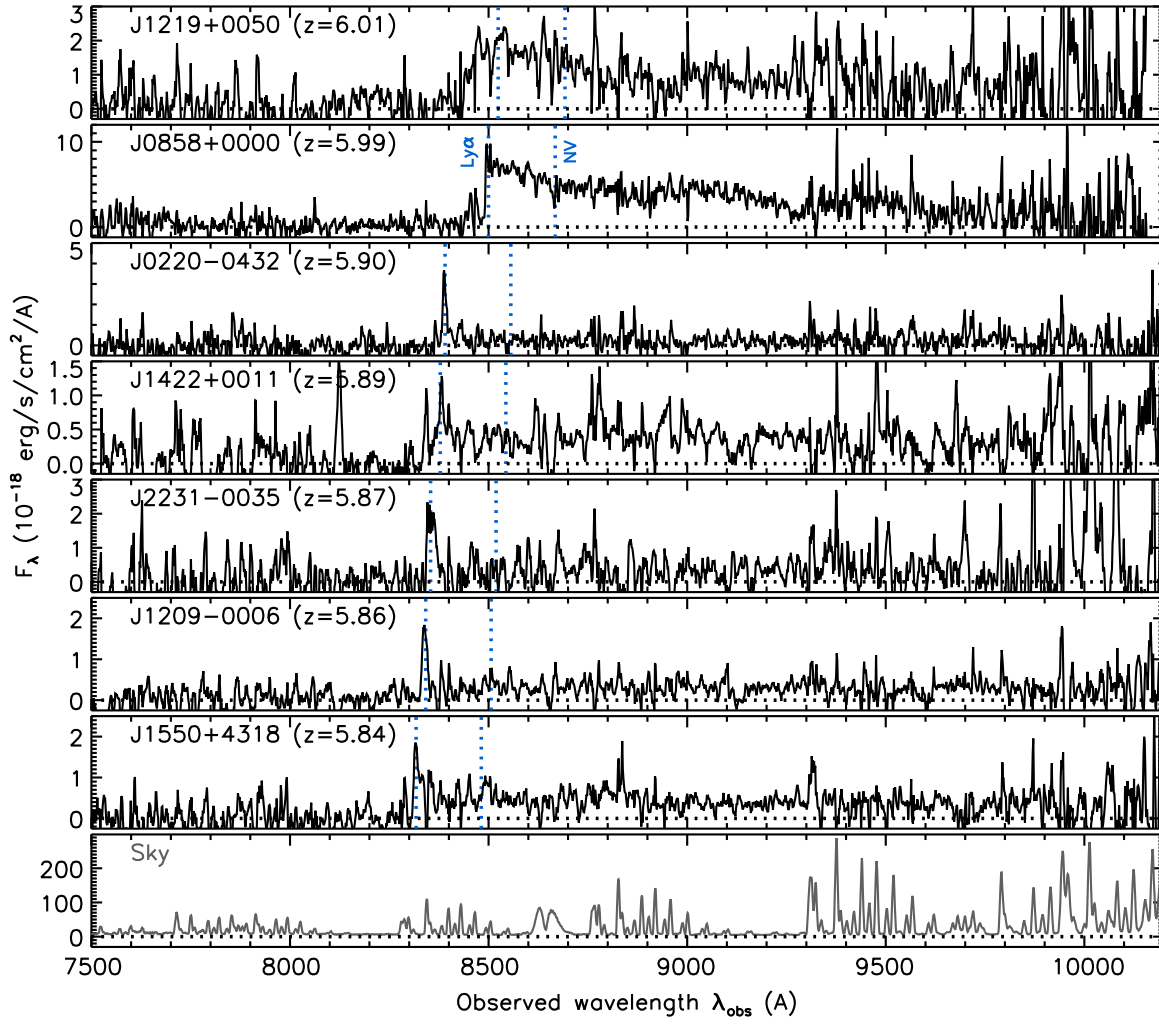


Figure 4. Same as Figure 1, but for the last set of seven quasars.

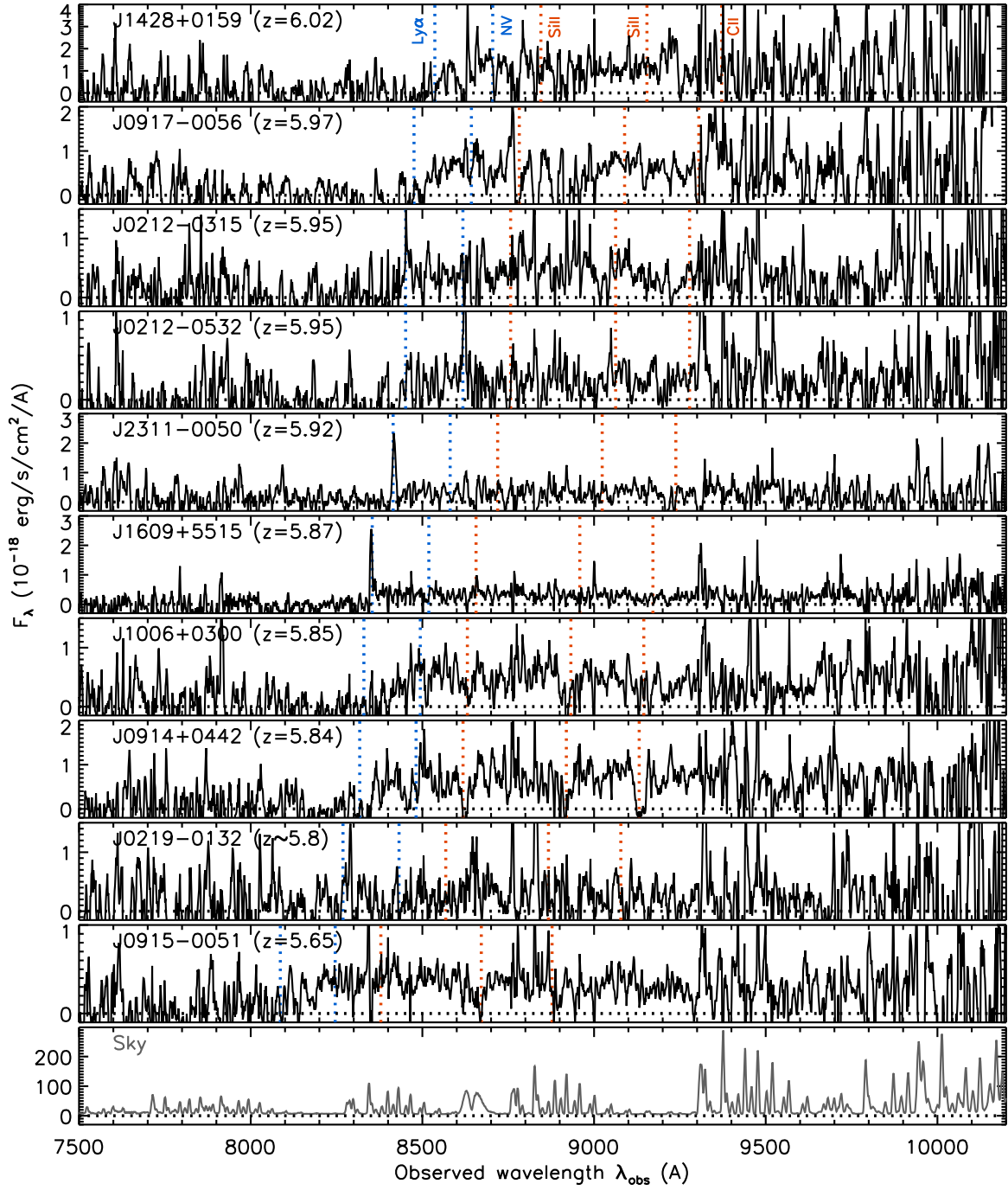


Figure 5. Same as Figure 1, but for the ten high- z galaxies. The expected positions of the interstellar absorption lines of Si II $\lambda 1260$, Si II $\lambda 1304$, and C II $\lambda 1335$ are marked by the red dotted lines.

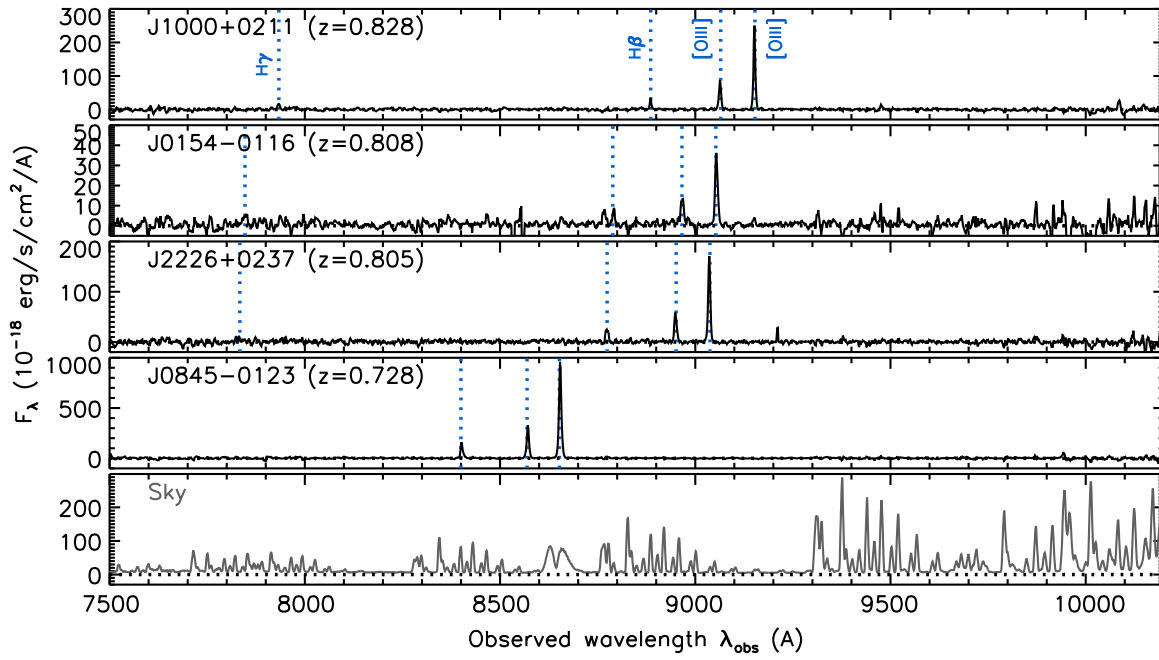


Figure 6. Same as Figure 1, but for the four [O III] emitters at $z \sim 0.8$. The expected positions of H γ , H β , and two [O III] lines (λ_{4959} and λ_{5007}) are marked by the dotted lines.

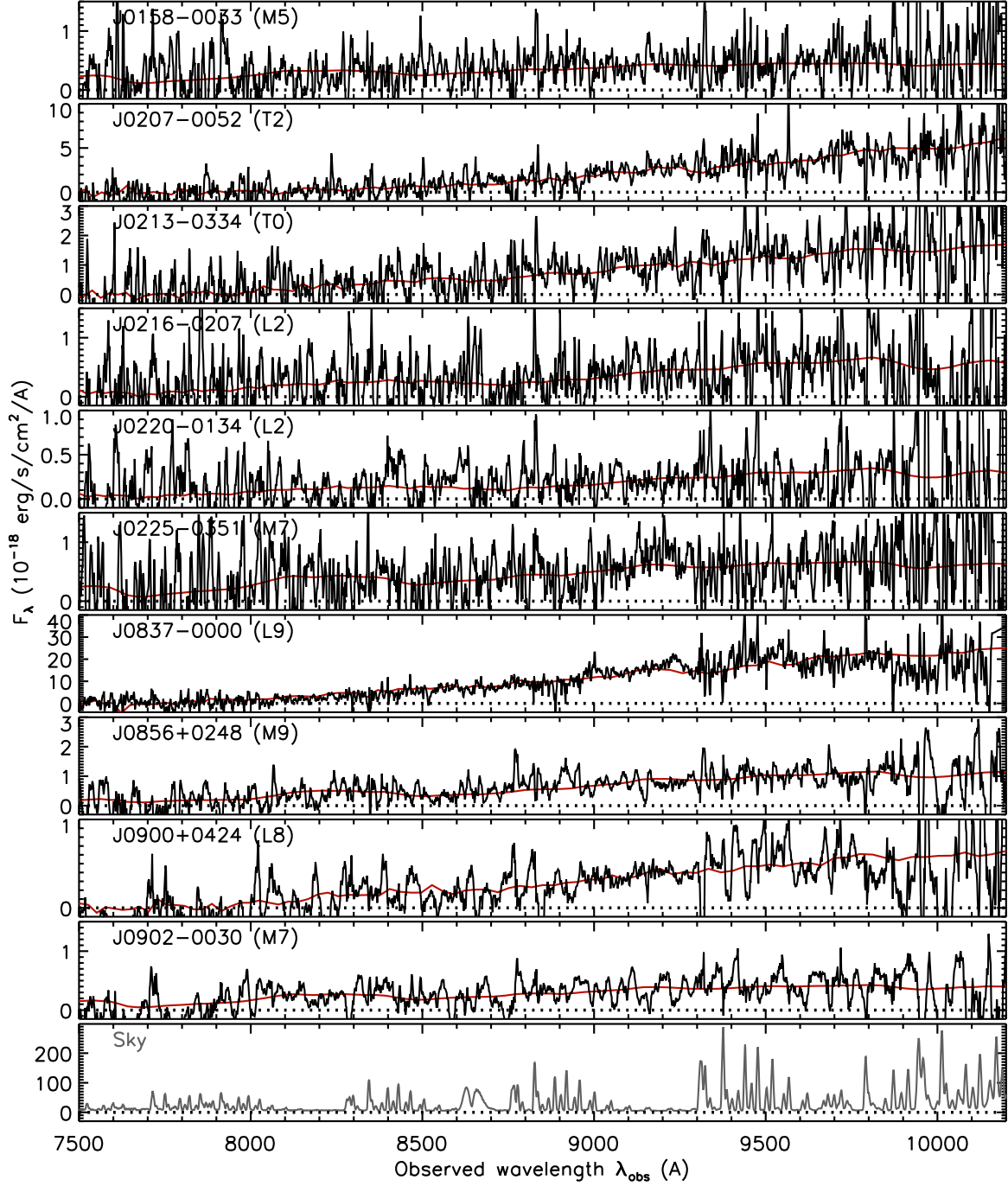


Figure 7. Same as Figure 1, but for the first set of ten cool dwarfs. The red lines represent the best-fit templates, whose spectral types are indicated at the top left corner of each panel. The small-scale ($<100 \text{ \AA}$) features seen in the spectra are due to noise, given the low S/N.

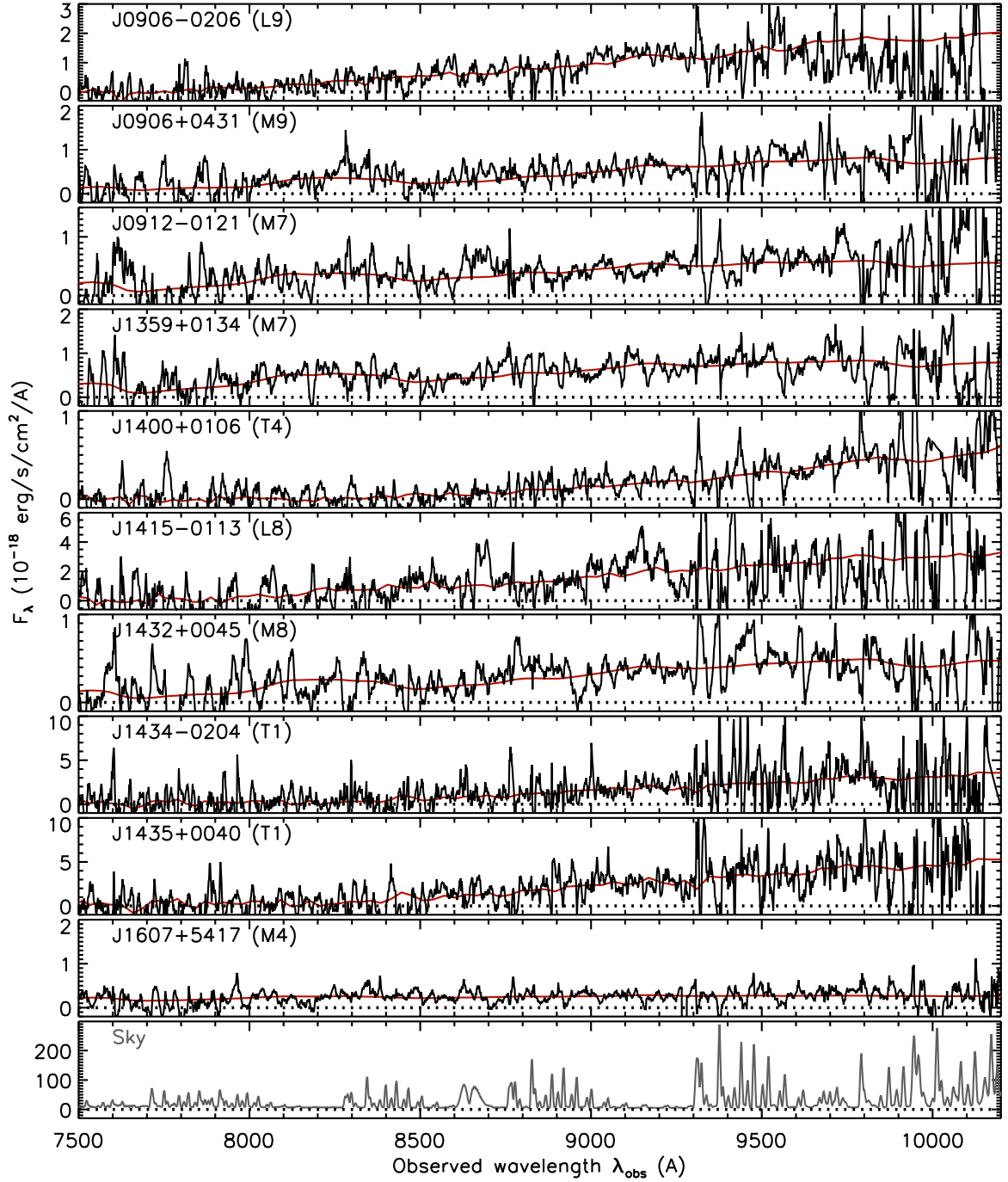


Figure 8. Same as Figure 7, but for the second set of ten cool dwarfs.

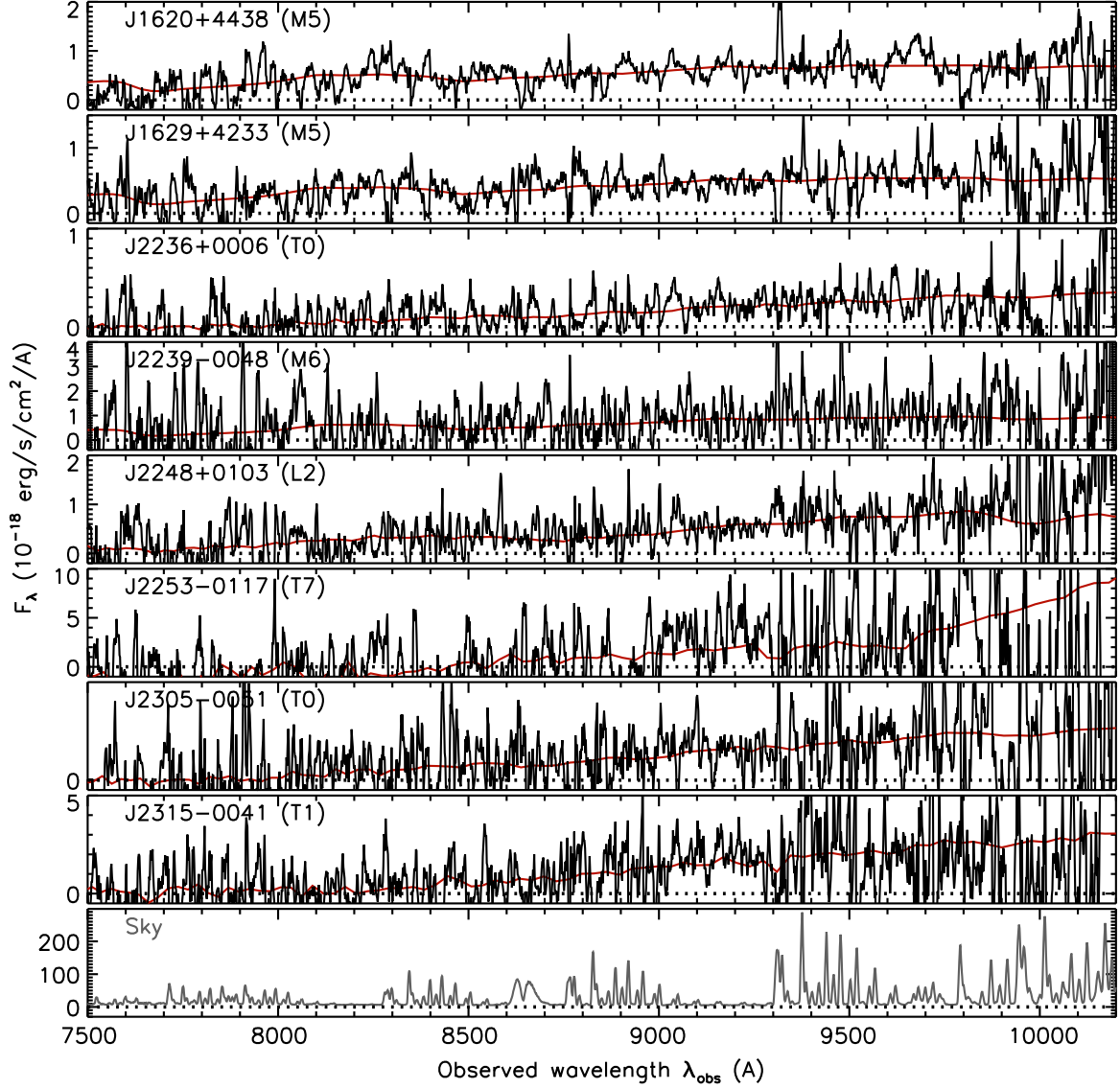


Figure 9. Same as Figure 7, but for the last set of eight cool dwarfs.

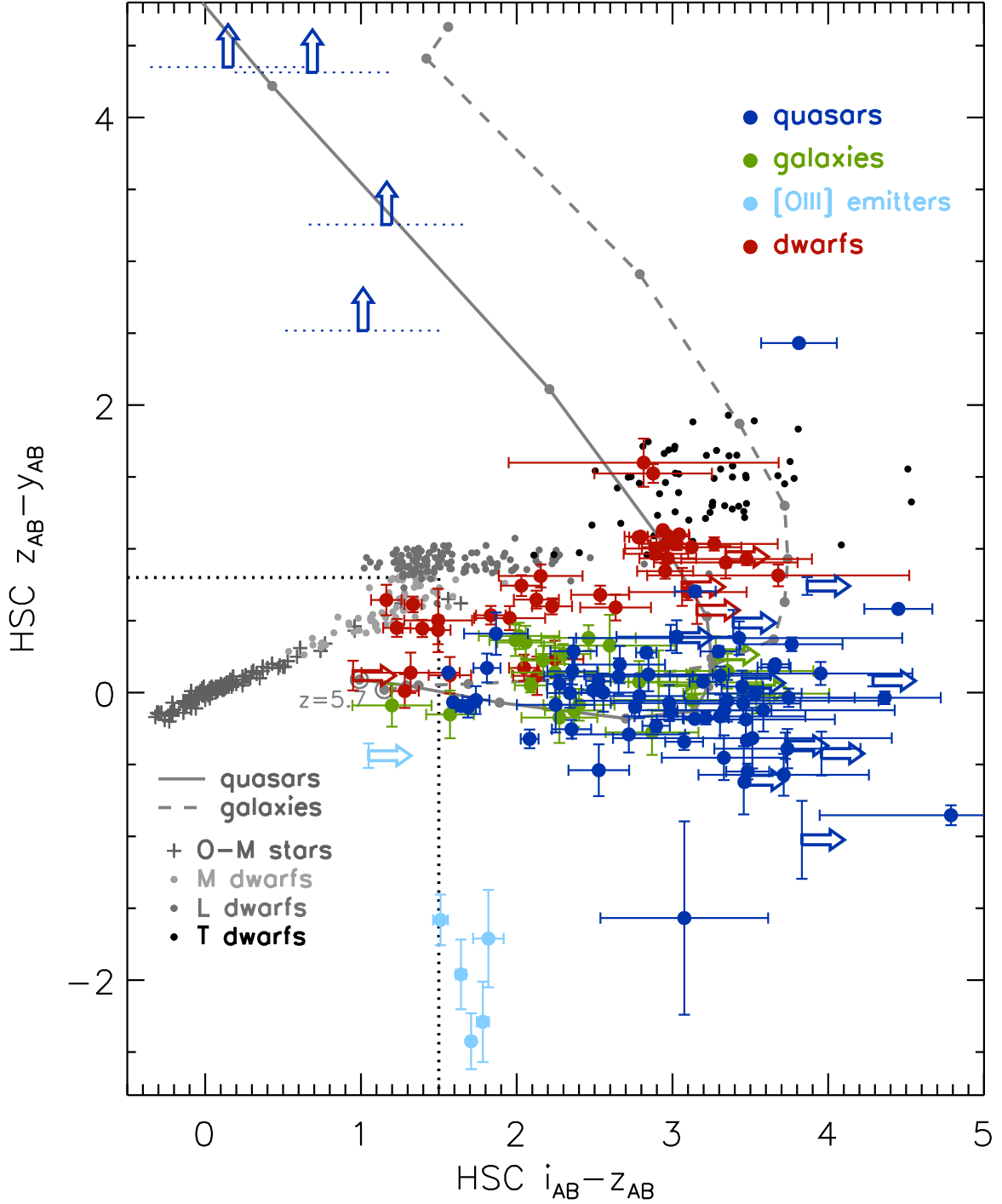


Figure 10. HSC $i_{AB} - z_{AB}$ and $z_{AB} - y_{AB}$ colors of the SHELLQs quasars (blue dots; including previously-known quasars we recovered), galaxies (green dots), [O III] emitters (light blue dots), and cool dwarfs (red dots). The grey crosses and dots represent Galactic stars (Pickles 1998) and brown dwarfs, while the solid and dashed lines represent models of quasars and galaxies at $z \geq 5.7$; the dots along the lines represent redshifts in steps of 0.1, with $z = 5.7$ marked by the large open circles. The dotted lines represent the color criteria used in our HSC database query. The four quasars at the top-left corner (marked by the up arrows) are undetected in the i and z bands, and are plotted at arbitrary horizontal positions. All the sources discovered in Paper I, II and this work are included.

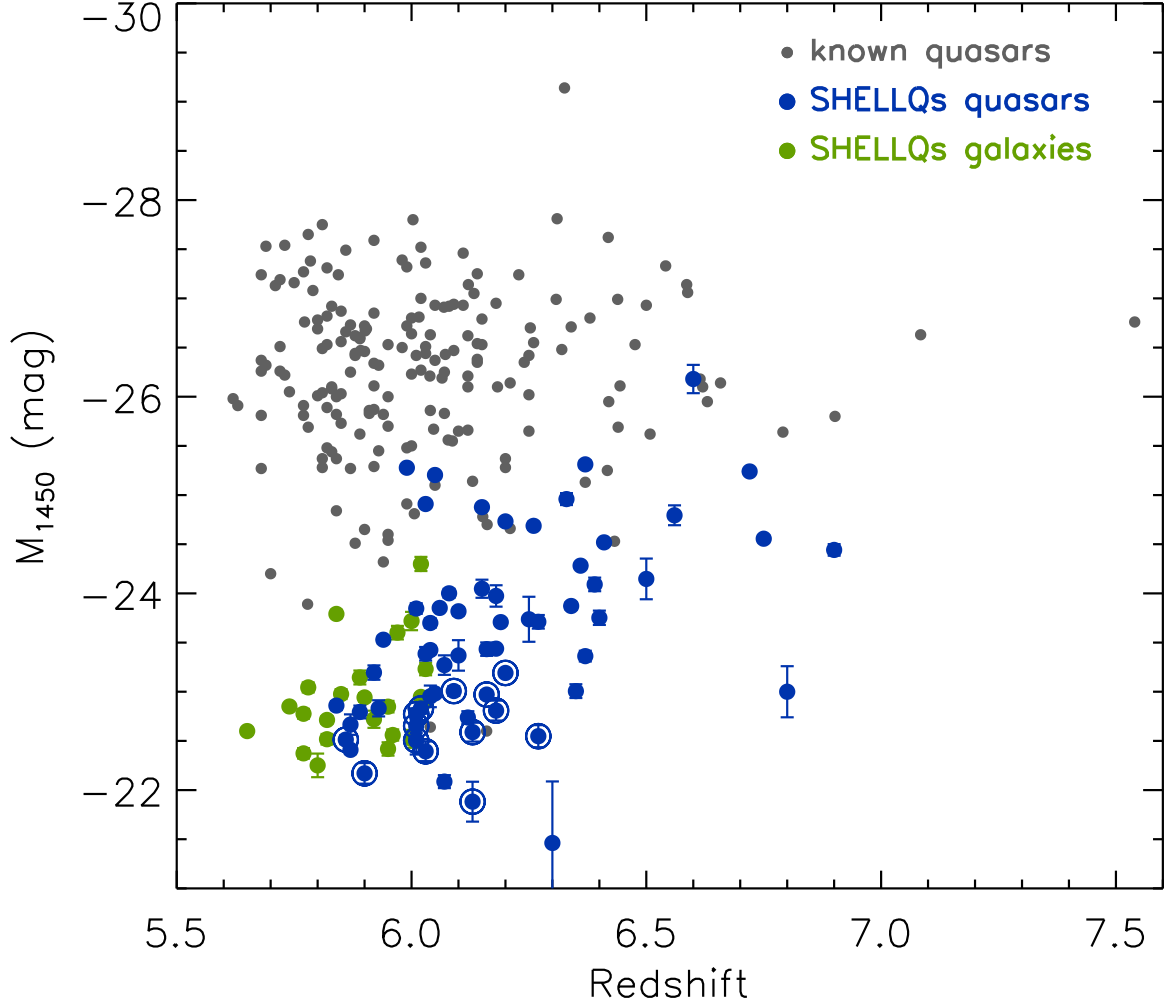


Figure 11. Rest-UV absolute magnitude at 1450 Å (M_{1450}), as a function of redshift, of the SHELLQs quasars (blue dots) and galaxies (green dots), as well as of all the high- z quasars discovered by other surveys and published to date (small grey dots). The SHELLQs quasars with narrow $\text{Ly}\alpha$ lines are marked with the larger circles. All the high- z objects discovered in Paper I, II, and this work are plotted.

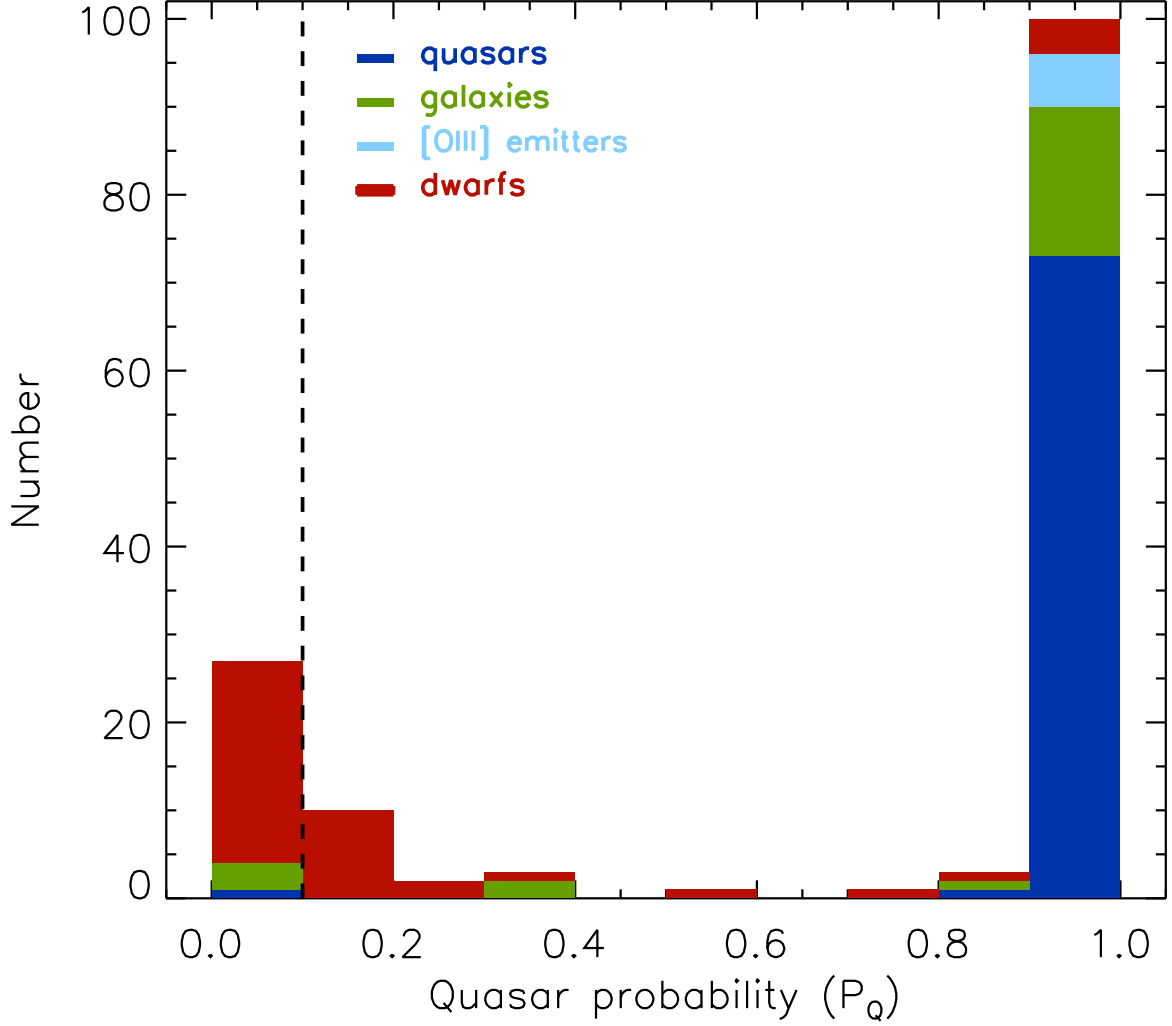


Figure 12. Histogram of the Bayesian quasar probability (P_Q^B) of the SHELLQs quasars (blue; including previously-known quasars we recovered), galaxies (green), [O III] emitters (light blue), and cool dwarfs (red). All the sources discovered in Paper I, II, and this work are counted. The dashed line represents our quasar selection threshold ($P_Q^B > 0.1$); there are objects below this threshold, because they had higher P_Q^B in the older HSC data releases.

Table 3. Photometric Properties

Name	R.A.	Decl.	i_{AB} (mag)	z_{AB} (mag)	y_{AB} (mag)	P_Q^B
Quasars						
<i>J</i> 2210 + 0304	22 ^h 10 ^m 27 ^s .24	+03°04′28″.5	27.36 ± 0.78	>25.03	22.94 ± 0.06	1.000
<i>J</i> 0213 − 0626	02 ^h 13 ^m 16 ^s .94	−06°26′15″.2	26.19 ± 0.30	>25.05	21.69 ± 0.03	1.000
<i>J</i> 0923 + 0402	09 ^h 23 ^m 47 ^s .12	+04°02′54″.4	26.45 ± 0.24	22.64 ± 0.02	20.21 ± 0.01	1.000
<i>J</i> 0921 + 0007	09 ^h 21 ^m 20 ^s .56	+00°07′22″.9	26.28 ± 0.22	21.83 ± 0.01	21.24 ± 0.01	1.000
<i>J</i> 1545 + 4232	15 ^h 45 ^m 05 ^s .62	+42°32′11″.6	25.74 ± 0.12	22.45 ± 0.01	22.16 ± 0.04	1.000
<i>J</i> 1004 + 0239	10 ^h 04 ^m 01 ^s .36	+02°39′30″.7	26.41 ± 0.11	22.76 ± 0.01	22.58 ± 0.01	1.000
<i>J</i> 0211 − 0203	02 ^h 11 ^m 44 ^s .53	−02°03′03″.9	27.47 ± 1.05	24.04 ± 0.06	23.66 ± 0.10	0.999
<i>J</i> 2304 + 0045	23 ^h 04 ^m 22 ^s .97	+00°45′05″.4	26.85 ± 0.33	23.08 ± 0.02	22.75 ± 0.04	1.000
<i>J</i> 2255 + 0251	22 ^h 55 ^m 38 ^s .04	+02°51′26″.6	>25.72	23.44 ± 0.05	22.95 ± 0.07	1.000
<i>J</i> 1406 − 0116	14 ^h 06 ^m 29 ^s .12	−01°16′11″.2	25.78 ± 0.13	22.64 ± 0.02	21.93 ± 0.03	1.000
<i>J</i> 1146 − 0005	11 ^h 46 ^m 58 ^s .89	−00°05′37″.7	>26.43	23.76 ± 0.04	24.78 ± 0.27	1.000
<i>J</i> 1146 + 0124	11 ^h 46 ^m 48 ^s .42	+01°24′20″.1	26.76 ± 0.42	23.01 ± 0.03	23.05 ± 0.06	1.000
<i>J</i> 0918 + 0139	09 ^h 18 ^m 33 ^s .17	+01°39′23″.3	26.70 ± 0.30	23.17 ± 0.03	23.18 ± 0.04	1.000
<i>J</i> 0844 − 0132	08 ^h 44 ^m 08 ^s .61	−01°32′16″.5	>26.24	23.31 ± 0.03	23.73 ± 0.15	1.000
<i>J</i> 1146 − 0154	11 ^h 46 ^m 32 ^s .66	−01°54′38″.3	26.90 ± 0.55	23.60 ± 0.06	23.76 ± 0.14	1.000
<i>J</i> 0834 + 0211	08 ^h 34 ^m 00 ^s .88	+02°11′46″.9	26.27 ± 0.32	22.97 ± 0.03	22.85 ± 0.05	1.000
<i>J</i> 0909 + 0440	09 ^h 09 ^m 21 ^s .50	+04°40′42″.9	25.02 ± 0.06	22.18 ± 0.02	21.91 ± 0.03	1.000
<i>J</i> 2252 + 0225	22 ^h 52 ^m 05 ^s .44	+02°25′31″.9	26.78 ± 0.37	23.80 ± 0.06	23.88 ± 0.11	1.000
<i>J</i> 1406 − 0144	14 ^h 06 ^m 46 ^s .88	−01°44′02″.6	26.78 ± 0.37	23.33 ± 0.04	23.40 ± 0.13	1.000
<i>J</i> 1416 + 0147	14 ^h 16 ^m 53 ^s .01	+01°47′02″.2	26.60 ± 0.55	22.89 ± 0.04	23.46 ± 0.14	1.000
<i>J</i> 0957 + 0053	09 ^h 57 ^m 40 ^s .39	+00°53′33″.6	>26.91	23.66 ± 0.01	23.58 ± 0.04	1.000
<i>J</i> 2223 + 0326	22 ^h 23 ^m 09 ^s .51	+03°26′20″.3	24.07 ± 0.03	21.31 ± 0.01	21.41 ± 0.02	1.000
<i>J</i> 1400 − 0125	14 ^h 00 ^m 29 ^s .99	−01°25′21″.0	25.16 ± 0.08	22.88 ± 0.02	22.82 ± 0.06	1.000
<i>J</i> 1400 − 0011	14 ^h 00 ^m 28 ^s .79	−00°11′51″.5	26.15 ± 0.19	23.62 ± 0.04	24.16 ± 0.18	1.000
<i>J</i> 1219 + 0050	12 ^h 19 ^m 05 ^s .34	+00°50′37″.5	24.90 ± 0.05	22.81 ± 0.02	23.13 ± 0.06	1.000
<i>J</i> 0858 + 0000	08 ^h 58 ^m 13 ^s .51	+00°00′57″.1	24.28 ± 0.04	21.29 ± 0.01	21.43 ± 0.01	1.000
<i>J</i> 0220 − 0432	02 ^h 20 ^m 29 ^s .72	−04°32′04″.0	26.29 ± 0.18	24.42 ± 0.10	24.01 ± 0.11	0.000
<i>J</i> 1422 + 0011	14 ^h 22 ^m 00 ^s .23	+00°11′03″.0	26.22 ± 0.14	23.85 ± 0.05	23.56 ± 0.08	1.000
<i>J</i> 2231 − 0035	22 ^h 31 ^m 48 ^s .89	−00°35′47″.5	26.52 ± 0.24	24.27 ± 0.07	24.35 ± 0.18	1.000
<i>J</i> 1209 − 0006	12 ^h 09 ^m 23 ^s .99	−00°06′46″.5	26.69 ± 0.23	24.13 ± 0.05	24.13 ± 0.12	1.000
<i>J</i> 1550 + 4318	15 ^h 50 ^m 00 ^s .93	+43°18′02″.8	25.52 ± 0.08	23.71 ± 0.03	23.54 ± 0.10	1.000
Galaxies						
<i>J</i> 1428 + 0159	14 ^h 28 ^m 24 ^s .71	+01°59′34″.4	26.05 ± 0.43	22.90 ± 0.05	22.83 ± 0.07	1.000
<i>J</i> 0917 − 0056	09 ^h 17 ^m 00 ^s .28	−00°56′58″.1	26.06 ± 0.18	23.69 ± 0.05	23.81 ± 0.10	1.000

Table 3 continued

Table 3 (*continued*)

Name	R.A.	Decl.	i_{AB} (mag)	z_{AB} (mag)	y_{AB} (mag)	P_Q^B
<i>J0212</i> − 0315	02 ^h 12 ^m 36 ^s .67	−03°15′17″.6	26.98 ± 0.50	23.85 ± 0.05	23.90 ± 0.13	1.000
<i>J0212</i> − 0532	02 ^h 12 ^m 49 ^s .46	−05°32′38″.0	>26.22	24.40 ± 0.08	24.31 ± 0.19	1.000
<i>J2311</i> − 0050	23 ^h 11 ^m 42 ^s .86	−00°50′20″.7	26.83 ± 0.41	24.23 ± 0.09	23.91 ± 0.20	0.356
<i>J1609</i> + 5515	16 ^h 09 ^m 52 ^s .79	+55°15′48″.5	25.89 ± 0.08	24.15 ± 0.03	24.20 ± 0.09	1.000
<i>J1006</i> + 0300	10 ^h 06 ^m 33 ^s .53	+03°00′05″.2	25.79 ± 0.10	23.70 ± 0.02	23.65 ± 0.05	1.000
<i>J0914</i> + 0442	09 ^h 14 ^m 36 ^s .47	+04°42′31″.7	25.46 ± 0.12	23.29 ± 0.06	23.07 ± 0.08	0.980
<i>J0219</i> − 0132	02 ^h 19 ^m 30 ^s .94	−01°32′07″.2	25.47 ± 0.24	24.27 ± 0.07	24.36 ± 0.13	0.820
<i>J0915</i> − 0051	09 ^h 15 ^m 45 ^s .02	−00°51′36″.0	25.61 ± 0.13	24.04 ± 0.08	24.19 ± 0.15	0.316
[O III] Emitters						
<i>J1000</i> + 0211	10 ^h 00 ^m 12 ^s .46	+02°11′27″.4	24.65 ± 0.04	22.87 ± 0.02	25.16 ± 0.28	1.000
<i>J0154</i> − 0116	01 ^h 54 ^m 31 ^s .69	−01°16′19″.5	>23.08	22.75 ± 0.04	23.19 ± 0.07	1.000
<i>J2226</i> + 0237	22 ^h 26 ^m 49 ^s .68	+02°37′54″.0	24.25 ± 0.03	22.61 ± 0.02	24.57 ± 0.24	1.000
<i>J0845</i> − 0123	08 ^h 45 ^m 16 ^s .54	−01°23′21″.6	23.59 ± 0.02	21.89 ± 0.01	24.31 ± 0.19	1.000
Cool Dwarfs						
<i>J0158</i> − 0033	01 ^h 58 ^m 07 ^s .10	−00°33′32″.1	>23.65	23.80 ± 0.07	23.68 ± 0.07	0.119
<i>J0207</i> − 0052	02 ^h 07 ^m 01 ^s .05	−00°52′25″.0	25.34 ± 0.32	22.22 ± 0.01	21.21 ± 0.01	0.831
<i>J0213</i> − 0334	02 ^h 13 ^m 50 ^s .82	−03°34′45″.2	25.99 ± 0.20	23.10 ± 0.03	22.10 ± 0.03	0.105
<i>J0216</i> − 0207	02 ^h 16 ^m 17 ^s .18	−02°07′19″.3	26.14 ± 0.26	23.99 ± 0.06	23.18 ± 0.06	0.000
<i>J0220</i> − 0134	02 ^h 20 ^m 47 ^s .41	−01°34′50″.6	25.73 ± 0.31	24.41 ± 0.08	24.27 ± 0.12	0.042
<i>J0225</i> − 0351	02 ^h 25 ^m 00 ^s .18	−03°51′46″.8	25.33 ± 0.08	23.50 ± 0.05	22.96 ± 0.05	0.000
<i>J0837</i> − 0000	08 ^h 37 ^m 17 ^s .18	−00°00′21″.0	23.18 ± 0.01	20.24 ± 0.01	19.11 ± 0.01	0.000
<i>J0856</i> + 0248	08 ^h 56 ^m 09 ^s .10	+02°48′51″.1	24.63 ± 0.12	23.24 ± 0.03	22.79 ± 0.05	0.000
<i>J0900</i> + 0424	09 ^h 00 ^m 18 ^s .40	+04°24′15″.5	27.46 ± 0.45	24.11 ± 0.08	23.21 ± 0.08	0.021
<i>J0902</i> − 0030	09 ^h 02 ^m 22 ^s .31	−00°30′40″.4	26.02 ± 0.22	24.07 ± 0.05	23.55 ± 0.07	0.000
<i>J0906</i> − 0206	09 ^h 06 ^m 50 ^s .82	−02°06′10″.2	25.06 ± 0.14	22.93 ± 0.05	22.29 ± 0.04	0.000
<i>J0906</i> + 0431	09 ^h 06 ^m 55 ^s .10	+04°31′31″.9	25.05 ± 0.06	23.56 ± 0.06	23.12 ± 0.08	0.000
<i>J0912</i> − 0121	09 ^h 12 ^m 10 ^s .99	−01°21′02″.9	>25.77	23.74 ± 0.07	23.17 ± 0.07	0.994
<i>J1359</i> + 0134	13 ^h 59 ^m 45 ^s .00	+01°34′12″.3	24.60 ± 0.07	23.32 ± 0.06	23.31 ± 0.10	0.533
<i>J1400</i> + 0106	14 ^h 00 ^m 15 ^s .38	+01°06′23″.7	27.91 ± 0.85	25.10 ± 0.15	23.50 ± 0.07	0.000
<i>J1415</i> − 0113	14 ^h 15 ^m 32 ^s .20	−01°13′14″.3	25.08 ± 0.06	22.30 ± 0.01	21.22 ± 0.01	0.000
<i>J1432</i> + 0045	14 ^h 32 ^m 05 ^s .78	+00°45′31″.7	25.59 ± 0.12	24.01 ± 0.07	23.89 ± 0.11	0.027
<i>J1434</i> − 0204	14 ^h 34 ^m 37 ^s .36	−02°04′16″.7	25.33 ± 0.18	22.36 ± 0.03	21.42 ± 0.02	0.000
<i>J1435</i> + 0040	14 ^h 35 ^m 29 ^s .69	+00°40′35″.3	25.17 ± 0.06	22.12 ± 0.01	21.02 ± 0.01	0.000
<i>J1607</i> + 5417	16 ^h 07 ^m 32 ^s .84	+54°17′24″.5	26.46 ± 0.12	24.23 ± 0.03	23.63 ± 0.05	0.295
<i>J1620</i> + 4438	16 ^h 20 ^m 46 ^s .91	+44°38′39″.7	25.64 ± 0.16	23.39 ± 0.09	23.16 ± 0.10	0.154
<i>J1629</i> + 4233	16 ^h 29 ^m 48 ^s .12	+42°33′38″.5	25.77 ± 0.09	23.72 ± 0.04	23.55 ± 0.08	1.000
<i>J2236</i> + 0006	22 ^h 36 ^m 12 ^s .42	+00°06′32″.6	26.27 ± 0.18	24.77 ± 0.13	24.27 ± 0.18	0.000

Table 3 continued

Table 3 (*continued*)

Name	R.A.	Decl.	i_{AB} (mag)	z_{AB} (mag)	y_{AB} (mag)	P_Q^B
<i>J2239</i> − 0048	22 ^h 39 ^m 53 ^s .43	−00°48′02″.6	24.23 ± 0.08	23.00 ± 0.04	22.55 ± 0.05	0.000
<i>J2248</i> + 0103	22 ^h 48 ^m 34 ^s .69	+01°03′12″.2	26.73 ± 0.38	23.63 ± 0.04	22.93 ± 0.04	0.997
<i>J2253</i> − 0117	22 ^h 53 ^m 57 ^s .80	−01°17′05″.3	25.65 ± 0.21	23.01 ± 0.08	22.42 ± 0.04	0.347
<i>J2305</i> − 0051	23 ^h 05 ^m 05 ^s .75	−00°51′32″.6	25.71 ± 0.13	23.58 ± 0.09	23.47 ± 0.10	0.719
<i>J2315</i> − 0041	23 ^h 15 ^m 14 ^s .06	−00°41′01″.1	25.69 ± 0.13	22.72 ± 0.02	21.63 ± 0.02	0.195

NOTE—Coordinates are at J2000.0. We took magnitudes from the latest HSC-SSP data release, and re-calculated P_Q^B for objects selected with the older data releases (this is why the quasar *J0220* − 0432 has $P_Q^B = 0.000$, which used to be higher in the old data release; see text). Magnitude upper limits are placed at 5σ significance.

Table 4. JHK magnitudes of the objects detected in UKIDSS or VIKING

Name	UKIDSS			VIKING		
	J_{AB} (mag)	H_{AB} (mag)	K_{AB} (mag)	J_{AB} (mag)	H_{AB} (mag)	K_{AB} (mag)
Quasars						
$J0923 + 0402$	20.02 ± 0.09	19.74 ± 0.16	19.32 ± 0.09
$J0921 + 0007$	20.90 ± 0.26	21.05 ± 0.15	...	20.38 ± 0.13
$J1406 - 0116$	22.06 ± 0.24
$J0858 + 0000$	21.19 ± 0.20	21.15 ± 0.20	21.18 ± 0.24
Cool Dwarfs						
$J0837 - 0000$	17.87 ± 0.01	17.63 ± 0.01	17.72 ± 0.01
$J0906 - 0206$	20.35 ± 0.22
$J0912 - 0121$	21.55 ± 0.31
$J1415 - 0113$	19.87 ± 0.16	19.67 ± 0.13	20.11 ± 0.21	20.07 ± 0.08	...	19.71 ± 0.08
$J1434 - 0204$	20.17 ± 0.19	20.44 ± 0.06	20.18 ± 0.10	20.19 ± 0.08
$J1435 + 0040$	19.75 ± 0.11	19.84 ± 0.13	19.86 ± 0.15	19.85 ± 0.03	19.68 ± 0.06	19.87 ± 0.06

Table 5. Spectroscopic Properties

Name	Redshift	M_{1450} (mag)	Line	EW_{rest} (\AA)	FWHM (km s^{-1})	$\log L$ (L in erg s^{-1})
Quasars						
<i>J</i> 2210 + 0304	6.9	-24.44 ± 0.06
<i>J</i> 0213 − 0626	6.72	-25.24 ± 0.02	Ly α	16 ± 1	1200 ± 100	44.18 ± 0.02
<i>J</i> 0923 + 0402	6.6	-26.18 ± 0.14
<i>J</i> 0921 + 0007	6.56	-24.79 ± 0.10	Ly α	170 ± 20	1400 ± 100	45.04 ± 0.01
<i>J</i> 1545 + 4232	6.50	-24.15 ± 0.21	Ly α	140 ± 30	960 ± 660	44.68 ± 0.03
<i>J</i> 1004 + 0239	6.41	-24.52 ± 0.03	Ly α	37 ± 2	2100 ± 300	44.27 ± 0.01
<i>J</i> 0211 − 0203	6.37	-23.36 ± 0.06	Ly α	26 ± 3	1200 ± 900	43.64 ± 0.04
<i>J</i> 2304 + 0045	6.36	-24.28 ± 0.03	Ly α	15 ± 1	710 ± 40	43.79 ± 0.03
<i>J</i> 2255 + 0251	6.34	-23.87 ± 0.04	Ly α	19 ± 2	1600 ± 300	43.72 ± 0.04
<i>J</i> 1406 − 0116	6.33	-24.96 ± 0.06
<i>J</i> 1146 − 0005	6.30	-21.46 ± 0.63	Ly α	260 ± 50	330 ± 100	44.18 ± 0.02
<i>J</i> 1146 + 0124	6.27	-23.71 ± 0.07	Ly α	57 ± 6	9700 ± 3700	44.12 ± 0.03
<i>J</i> 0918 + 0139	6.19	-23.71 ± 0.04	Ly α	23 ± 2	6200 ± 1700	43.74 ± 0.04
<i>J</i> 0844 − 0132	6.18	-23.97 ± 0.11	Ly α	57 ± 6	1600 ± 300	44.25 ± 0.02
<i>J</i> 1146 − 0154	6.16	-23.43 ± 0.07	Ly α	7.3 ± 4.0	1600 ± 400	43.13 ± 0.23
<i>J</i> 0834 + 0211	6.15	-24.05 ± 0.09	Ly α	16 ± 4	4900 ± 800	43.72 ± 0.10
<i>J</i> 0909 + 0440	6.15	-24.88 ± 0.02
<i>J</i> 2252 + 0225	6.12	-22.74 ± 0.06	Ly α	47 ± 5	2200 ± 600	43.65 ± 0.04
<i>J</i> 1406 − 0144	6.10	-23.37 ± 0.16	Ly α	68 ± 8	1600 ± 500	44.00 ± 0.03
<i>J</i> 1416 + 0147	6.07	-23.27 ± 0.10	Ly α	68 ± 7	2300 ± 200	44.03 ± 0.03
<i>J</i> 0957 + 0053	6.05	-22.98 ± 0.04	Ly α	26 ± 4	2200 ± 1500	43.48 ± 0.06
<i>J</i> 2223 + 0326	6.05	-25.20 ± 0.02	Ly α	37 ± 2	4700 ± 3500	44.53 ± 0.02
<i>J</i> 1400 − 0125	6.04	-23.70 ± 0.05	Ly α	28 ± 4	12000 ± 4000	43.80 ± 0.05
<i>J</i> 1400 − 0011	6.04	-22.95 ± 0.11	Ly α	56 ± 3	620 ± 60	43.84 ± 0.01
<i>J</i> 1219 + 0050	6.01	-23.85 ± 0.05	Ly α	26 ± 4	7500 ± 4400	43.84 ± 0.06
<i>J</i> 0858 + 0000	5.99	-25.28 ± 0.01	Ly α	24 ± 1	11000 ± 1000	44.38 ± 0.01
<i>J</i> 0220 − 0432	5.90	-22.17 ± 0.10	Ly α	29 ± 2	< 230	43.15 ± 0.03
<i>J</i> 1422 + 0011	5.89	-22.79 ± 0.07	Ly α	7.2 ± 1.7	980 ± 360	42.82 ± 0.10
<i>J</i> 2231 − 0035	5.87	-22.67 ± 0.10	Ly α	21 ± 3	790 ± 250	43.23 ± 0.05
<i>J</i> 1209 − 0006	5.86	-22.51 ± 0.05	Ly α	26 ± 5	580 ± 50	43.01 ± 0.04
<i>J</i> 1550 + 4318	5.84	-22.86 ± 0.04	Ly α	4.8 ± 1.5	2600 ± 100	42.70 ± 0.13
Galaxies						
<i>J</i> 1428 + 0159	6.02	-24.30 ± 0.07

Table 5 continued

Table 5 (*continued*)

Name	Redshift	M_{1450} (mag)	Line	EW_{rest} (Å)	FWHM (km s $^{-1}$)	$\log L$ (L in erg s $^{-1}$)
<i>J0917</i> – 0056	5.97	-23.60 ± 0.07
<i>J0212</i> – 0315	5.95	-22.85 ± 0.06	Ly α	5.0 ± 1.0	650 ± 50	42.69 ± 0.09
<i>J0212</i> – 0532	5.95	-22.42 ± 0.07
<i>J2311</i> – 0050	5.92	-22.72 ± 0.09	Ly α	10 ± 1	250 ± 90	42.89 ± 0.04
<i>J1609</i> + 5515	5.87	-22.41 ± 0.04	Ly α	9.1 ± 0.6	480 ± 260	42.81 ± 0.03
<i>J1006</i> + 0300	5.85	-22.98 ± 0.05
<i>J0914</i> + 0442	5.84	-23.79 ± 0.04
<i>J0219</i> – 0132	5.8	-22.25 ± 0.12
<i>J0915</i> – 0051	5.65	-22.60 ± 0.03
[O III] Emitters						
<i>J1000</i> + 0211	0.828	...	H γ	370 ± 120	< 230	41.67 ± 0.03
		...	H β	860 ± 290	< 230	42.04 ± 0.03
		...	[OIII] $\lambda 4959$	2000 ± 700	< 230	42.41 ± 0.01
		...	[OIII] $\lambda 5007$	6000 ± 2000	< 230	42.88 ± 0.01
<i>J0154</i> – 0116	0.808	...	H γ	58 ± 14	410 ± 290	41.23 ± 0.10
		...	H β	85 ± 13	< 230	41.39 ± 0.05
		...	[OIII] $\lambda 4959$	130 ± 18	240 ± 140	41.57 ± 0.04
		...	[OIII] $\lambda 5007$	320 ± 30	< 230	41.96 ± 0.02
<i>J2226</i> + 0237	0.805	...	H γ	120 ± 20	390 ± 40	41.50 ± 0.05
		...	H β	270 ± 50	270 ± 50	41.86 ± 0.03
		...	[OIII] $\lambda 4959$	480 ± 80	< 230	42.11 ± 0.01
		...	[OIII] $\lambda 5007$	1400 ± 200	< 230	42.59 ± 0.01
<i>J0845</i> – 0123	0.728	...	H γ
		...	H β	680 ± 70	< 230	42.52 ± 0.01
		...	[OIII] $\lambda 4959$	1600 ± 200	< 230	42.89 ± 0.01
		...	[OIII] $\lambda 5007$	4700 ± 500	< 230	43.37 ± 0.01

NOTE—Redshifts are recorded to two significant figures when the position of Ly α emission or interstellar absorption is unambiguous.

5. SUMMARY

This paper is the fourth in a series presenting the results from the SHELLQs project, a search for low-luminosity quasars at $z \gtrsim 6$ based on the deep multi-band imaging data produced by the HSC-SSP survey. We continue to use the quasar selection procedure we described in Paper I and II, and here report spectroscopy of additional objects that roughly double the number of identifications compared to previous papers. Through the SHELLQs project, we have so far identified 137 extremely red HSC sources over about 650 deg 2 , which

include 64 high- z quasars, 24 high- z luminous galaxies, 6 [O III] emitters at $z \sim 0.8$, and 43 Galactic cool dwarfs. Our discovery now exceeds, in number, the final SDSS sample of 52 high- z quasars (Jiang et al. 2016). The new quasars span luminosities from $M_{1450} \sim -26$ to -22 mag, and continue to probe a few magnitude lower luminosities than have been probed by previous wide-field surveys. Our companion paper will present the quasar luminosity function established over an unprecedentedly wide range of $M_{1450} \sim -28$ to -21 mag, using the SHELLQs and other survey outcomes.

Table 6. Spectral classes of the cool dwarfs

Name	Class
<i>J0158 – 0033</i>	M5
<i>J0207 – 0052</i>	T2
<i>J0213 – 0334</i>	T0
<i>J0216 – 0207</i>	L2
<i>J0220 – 0134</i>	L2
<i>J0225 – 0351</i>	M7
<i>J0837 – 0000</i>	L9
<i>J0856 + 0248</i>	M9
<i>J0900 + 0424</i>	L8
<i>J0902 – 0030</i>	M7
<i>J0906 – 0206</i>	L9
<i>J0906 + 0431</i>	M9
<i>J0912 – 0121</i>	M7
<i>J1359 + 0134</i>	M7
<i>J1400 + 0106</i>	T4
<i>J1415 – 0113</i>	L8
<i>J1432 + 0045</i>	M8
<i>J1434 – 0204</i>	T1
<i>J1435 + 0040</i>	T1
<i>J1607 + 5417</i>	M4
<i>J1620 + 4438</i>	M5
<i>J1629 + 4233</i>	M5
<i>J2236 + 0006</i>	T0
<i>J2239 – 0048</i>	M6
<i>J2248 + 0103</i>	L2
<i>J2253 – 0117</i>	T7
<i>J2305 – 0051</i>	T0
<i>J2315 – 0041</i>	T1

NOTE—These classification should be regarded as only approximate; see text.

Our project will continue to identify high- z quasars in the HSC data, as the SSP survey continues toward its goal of observing $1,400 \text{ deg}^2$ in the Wide layer, and 27 and 3.5 deg^2 in the Deep and UltraDeep layers, respectively. At the same time, we are carrying out

multi-wavelength follow-up observations of the discovered objects. Black hole masses are being measured with Mg II $\lambda 2800$ lines obtained with near-IR spectrographs on Subaru, the Gemini telescopes, and the Very Large Telescope (M. Onoue et al., in prep.). We are also using ALMA, in order to probe the stellar and gaseous properties of the host galaxies (partly published in Izumi et al. 2018). The results of these observations will be presented in forthcoming papers.

This work is based on data collected at the Subaru Telescope, which is operated by the National Astronomical Observatory of Japan (NAOJ). We appreciate the staff members of the telescope for their support during our FOCAS observations. The data analysis was in part carried out on the open use data analysis computer system at the Astronomy Data Center of NAOJ.

This work is also based on observations made with the Gran Telescopio Canarias (GTC), installed at the Spanish Observatorio del Roque de los Muchachos of the Instituto de Astrofísica de Canarias, on the island of La Palma. We thank Stefan Geier and other support astronomers for their help during preparation and execution of our observing program.

YM was supported by the Japan Society for the Promotion of Science (JSPS) KAKENHI Grant No. JP17H04830.

The Hyper Suprime-Cam (HSC) collaboration includes the astronomical communities of Japan and Taiwan, and Princeton University. The HSC instrumentation and software were developed by NAOJ, the Kavli Institute for the Physics and Mathematics of the Universe (Kavli IPMU), the University of Tokyo, the High Energy Accelerator Research Organization (KEK), the Academia Sinica Institute for Astronomy and Astrophysics in Taiwan (ASIAA), and Princeton University. Funding was contributed by the FIRST program from Japanese Cabinet Office, the Ministry of Education, Culture, Sports, Science and Technology (MEXT), the Japan Society for the Promotion of Science (JSPS), Japan Science and Technology Agency (JST), the Toray Science Foundation, NAOJ, Kavli IPMU, KEK, ASIAA, and Princeton University.

This paper makes use of software developed for the Large Synoptic Survey Telescope (LSST). We thank the LSST Project for making their code available as free software at <http://dm.lsst.org>.

The Pan-STARRS1 Surveys (PS1) have been made possible through contributions of the Institute for Astronomy, the University of Hawaii, the Pan-STARRS Project Office, the Max-Planck Society and its participating institutes, the Max Planck Institute for As-

tronomy, Heidelberg and the Max Planck Institute for Extraterrestrial Physics, Garching, The Johns Hopkins University, Durham University, the University of Edinburgh, Queen's University Belfast, the Harvard-Smithsonian Center for Astrophysics, the Las Cumbres Observatory Global Telescope Network Incorporated, the National Central University of Taiwan, the Space Telescope Science Institute, the National Aeronautics and Space Administration under Grant No. NNX08AR22G issued through the Planetary Science Di-

vision of the NASA Science Mission Directorate, the National Science Foundation under Grant No. AST-1238877, the University of Maryland, Eötvös Lorand University (ELTE) and the Los Alamos National Laboratory.

IRAF is distributed by the National Optical Astronomy Observatory, which is operated by the Association of Universities for Research in Astronomy (AURA) under a cooperative agreement with the National Science Foundation.

REFERENCES

- Abazajian, K., Adelman-McCarthy, J. K., Agüeros, M. A., et al. 2004, *AJ*, 128, 502
- Aihara, H., Armstrong, R., Bickerton, S., et al. 2018, *PASJ*, 70, S8
- Aihara, H., Arimoto, N., Armstrong, R., et al. 2018, *PASJ*, 70, S4
- Bañados, E., Venemans, B. P., Mazzucchelli, C., et al. 2018, *Nature*, 553, 473
- Bañados, E., Venemans, B. P., Decarli, R., et al. 2016, *ApJS*, 227, 11
- Bertin, E., & Arnouts, S. 1996, *A&AS*, 117, 393
- Bosch, J., Armstrong, R., Bickerton, S., et al. 2018, *PASJ*, 70, S5
- Burgasser, A. J. 2014, *Astronomical Society of India Conference Series*, 11,
- Caballero, J. A., Burgasser, A. J., & Klement, R. 2008, *A&A*, 488, 181
- Cardamone, C., Schawinski, K., Sarzi, M., et al. 2009, *MNRAS*, 399, 1191
- Cepa, J., Aguiar, M., Escalera, V. G., et al. 2000, *Proc. SPIE*, 4008, 623
- Decarli, R., Walter, F., Venemans, B. P., et al. 2017, *Nature*, 545, 457
- Fan, X., Carilli, C. L., & Keating, B. 2006, *ARA&A*, 44, 415
- Ferrara, A., Salvadori, S., Yue, B., & Schleicher, D. 2014, *MNRAS*, 443, 2410
- Fukugita, M., Ichikawa, T., Gunn, J. E., et al. 1996, *AJ*, 111, 1748
- Furusawa, H., Koike, M., Takata, T., et al. 2018, *PASJ*, 70, S3
- Goto, T., Utsumi, Y., Furusawa, H., Miyazaki, S., & Komiyama, Y. 2009, *MNRAS*, 400, 843
- Gunn, J. E., & Peterson, B. A. 1965, *ApJ*, 142, 1633
- Izumi, T., Onoue, M., Shirakata, H., et al. 2018, *arXiv:1802.05742* (Paper III)
- Jarvis, M. J., Bonfield, D. G., Bruce, V. A., et al. 2013, *MNRAS*, 428, 1281
- Jiang, L., McGreer, I. D., Fan, X., et al. 2016, *ApJ*, 833, 222
- Jurić, M., Kantor, J., Lim, K., et al. 2015, *arXiv:1512.07914*
- Kashikawa, N., Aoki, K., Asai, R., et al. 2002, *PASJ*, 54, 819
- Kewley, L. J., Yuan, T., Nanayakkara, T., et al. 2016, *ApJ*, 819, 100
- Komiyama, Y., Obuchi, Y., Nakaya, H., et al. 2018, *PASJ*, 70, S2
- Konno, A., Ouchi, M., Nakajima, K., et al. 2016, *ApJ*, 823, 20
- Lawrence, A., Warren, S. J., Almaini, O., et al. 2007, *MNRAS*, 379, 1599
- Madau, P., Haardt, F., & Dotti, M. 2014, *ApJL*, 784, L38
- Matsuoka, Y., Onoue, M., Kashikawa, N., et al. 2016, *ApJ*, 828, 26 (Paper I)
- Matsuoka, Y., Onoue, M., Kashikawa, N., et al. 2018, *PASJ*, 70, S35 (Paper II)
- McCracken, H. J., Milvang-Jensen, B., Dunlop, J., et al. 2012, *A&A*, 544, A156
- Miyazaki, S., Komiyama, Y., Kawanomoto, S., et al. 2018, *PASJ*, 70, S1
- Mortlock, D. J., Warren, S. J., Venemans, B. P., et al. 2011, *Nature*, 474, 616
- Oke, J. B., & Gunn, J. E. 1983, *ApJ*, 266, 713
- Pickles, A. J. 1998, *PASP*, 110, 863
- Richards, G. T., Fan, X., Newberg, H. J., et al. 2002, *AJ*, 123, 2945
- Schlegel, D. J., Finkbeiner, D. P., & Davis, M. 1998, *ApJ*, 500, 525
- Songaila, A. 2004, *AJ*, 127, 2598
- Stanway, E. R., McMahon, R. G., & Bunker, A. J. 2005, *MNRAS*, 359, 1184
- Skrzypek, N., Warren, S. J., Faherty, J. K., et al. 2015, *A&A*, 574, A78

- Vanden Berk, D. E., Richards, G. T., Bauer, A., et al. 2001, AJ, 122, 549
- Volonteri, M. 2012, Science, 337, 544
- Willott, C. J., Delfosse, X., Forveille, T., Delorme, P., & Gwyn, S. D. J. 2005, ApJ, 633, 630
- Willott, C. J., Delorme, P., Reyl  , C., et al. 2010b, AJ, 139, 906